

**RESPONSE OF TROPICAL CLOUDS TO THE INTERANNUAL
VARIATION OF SEA SURFACE TEMPERATURE**

Rong Fu¹, W. Timothy Liu², and Robert E. Dickinson

¹Institute of Atmospheric Physics

The University of Arizona

Tucson, AZ 85721

²Jet Propulsion Laboratory

California Institute of Technology

Pasadena, CA 91109

revised for Journal of Climate
August 4, 1995

¹ Corresponding author address: Dr. Rong Fu, Institute of Atmospheric Physics, The University of Arizona, PAS
Building #81, Tucson, AZ 85721.

Abstract

Connection between the large-scale inter-annual variations of clouds, deep convection, atmospheric winds and **vertical** thermodynamic structure and SST over global tropical oceans are examined over the period **July 1983 - December 1990**. The SST warming associated with El Niño had a significant impact on the global tropical **cloud field** although the warming itself was confined to the equatorial central and eastern **Pacific**. Extensive variations of the total cloud field occurred in the northeastern Indian, western and central Pacific and western **Atlantic** oceans. The changes of high and middle clouds dominated the total cloud variation in these regions. Total cloud variation was relatively weak in the eastern Pacific and Atlantic because of the cancellation between the changes of high and low clouds. The variation of low clouds dominated the **total** cloud change in those areas.

The destabilization of the lapse rate between 900mb and 750 mb was more important for enhancing convective instability than was the change of local SST in the equatorial central Pacific during 1987 El Niño. This destabilization is associated with anomalous rising motion in that region. As a result, convection and high and middle clouds increased in the equatorial central Pacific. In the subtropical Pacific, both the change of lapse rate between 900 mb and 750 mb associated with anomalous subsidence and the decrease of **boundary** layer buoyancy due to decrease of temperature and **moisture** played an important role in enhancing convective stability. Consequently, convection, as well as high and middle clouds, **decreased** in these areas. The change of low clouds in the equatorial and south eastern Atlantic was correlated to both local SST and the SST changes in the equatorial eastern Pacific. In this area, the increase of low clouds was consistent with the sharper inversion during 1987 El Niño. The strengthening of the inversion was not caused by a local SST change although the local SST change appeared to be correlated to the change of low clouds.

The coherence between clouds and SST tendency shows that SST tendency leads cloud variation in the equatorial Pacific. Thus, the change of clouds does not dominate the sign of SST tendency even though the cloud change was maximum during 1987 El Niño. In some areas of the Indian, subtropical Pacific and north Atlantic oceans, cloud change leads SST tendency. Cloud change might affect SST tendency in these regions.

1. Introduction

On a global scale, cloud feedbacks have long been **identified** as the largest source of uncertainty for using climate models to project the response to increasing greenhouse gases. This assessment has been reinforced by international model **intercomparisons** (i.e. Cess et al. 1990) of the sensitivity of a wide variety of climate models to uniform increments of the ocean sea-surface temperature (SST). The large spread found between models for the inferred sensitivity has been shown to be almost entirely a result of different feedbacks between these different models. Indeed a wide range of feedbacks is possible simply through changes of the treatment of cloud microphysics and radiative properties (Senior and **Mitchell** 1993). However, the **global** effects of clouds are comprised of the average of a large number of **regional** cloud processes. On a regional and local scale, the occurrence and properties of clouds depend also on complex dynamic and thermodynamic couplings between the surface and atmosphere. Although not yet examined, it is likely that these regional cloud processes also vary **widely** between existing climate models because of their dependence on different treatments of surface and boundary layer processes, of moist convection, and of the interactions of these with **radiative** and **microphysical** properties of the clouds.

A good source of observational information to examine regional cloud feedback processes is the large-scale, **interannual** variations of SST in the tropical Pacific that affect global atmospheric circulation, associated with the El Niño-Southern Oscillation (ENSO). Over the tropical oceans, changes in SST have long been identified as an important mechanism for the forcing of clouds. They can do so directly by changing the humidity and thermodynamic properties of the boundary layer which supplies moisture to clouds. How the overlying atmosphere column above **the** boundary layer responds to these changes, however, depends on its profiles of temperature and **humidity**. If it is stable to deep convection, it may only respond through changes of its boundary layer. On the other hand, **if** deep convection does occur, it can have a profound effect on processes elsewhere, through the large mass and **moisture** movements that it implies. Vertical exchange can lead to high cirrus clouds. Horizontal exchange can lead to

changes in the convergence of moisture in remote boundary layers, and to increased subsidence stabilization. These changes and their effects on convection in remote areas can link back to the column initially under consideration and in turn modify its stability to further moist convection. It is the possibility of these dynamical linkages that makes the question of cloud feedbacks on a regional scale especially complex. Further complexity is added by the effects of clouds on surface radiation and hence the possibility that cloud changes will, in turn, feedback on SSTs and either modify the local change or force remote changes through the remote cloud responses. An understanding of all these coupling processes would show how clouds contribute to annual and interannual changes over the tropical oceans and help identify the processes important for the occurrence of clouds.

How interannual changes in SSTs are related to cloud-radiative flux changes has been much discussed (Ramanathan and Collins 1991; Heymsfield and Miloshevich 1991; Wallace 1992; Fu et al. 1992; Stephens and Slingo 1992; Hartmann and Michelsen 1993; Waliser and Graham 1993; Washington and Meehl 1993; Lau et al. 1994; Pierrehumbert 1995). Coupled ocean-atmosphere models with prescribed climatological SSTs have been able to predict the interannual changes in SSTs to first order approximation without cloud feedback effects on SST (e.g., Zebiak and Cane 1987). Correctly including these cloud processes, however, would provide a more accurate prediction of ENSO (Seager and Blumenthal 1995; Waliser et al. 1993). Because ENSO is dynamically driven, clouds may affect variations of tropical SSTs on ENSO scales differently than they affect time mean SSTs or changes on longer time scales. Modeling the seasonal cycle of SSTs also requires a description of cloud effects on surface radiation.

What are the physical causes of the observed correlations between clouds and SSTs? Answering this question would help determine how cloud feedbacks affect the ocean-atmosphere system. For example, a change of cloud forcing of -27 W m^{-2} to -22 W m^{-2} per degree C (Ramanathan and Collins 1991) has been observed at the equatorial Pacific during the 1987 El Niño. Based on this correlation, Ramanathan and Collins concluded that cloud feedback would provide a very strong, negative feedback to the changes in tropical SSTs; and consequently, that

cloud feedback should be responsible for the stabilization of SSTs. However, other studies have shown that the cloud changes associated with ENSO are more directly caused by the change of atmospheric circulation (Fu et al. 1992; Stephen and Slingo 1992; Hartmann and Michelson 1993; Lau et al. 1994), so that the range of -27 to -22 W m⁻² overestimates the cloud feedback.

Our research emphasizes distinguishing between the effects of SST anomalies and circulation changes on the cloud field. Total cloud cover is determined by different cloud types that are associated with various thermal and dynamic processes and may respond to the same SST perturbation in different ways. Thus, we study the different cloud types separately to clarify the links between cloud changes and atmospheric processes. Previous studies of this question have examined the behavior of cirrus/anvil clouds (Fu et al. 1992; Lau et al. 1994) and convective clouds (Waliser and Graham 1993), but did not explore, whether other clouds, especially low clouds, are also important for the total cloud variations over tropical oceans. While this analysis by itself provides no direct insights into the question of global cloud feedbacks, it should help prevent the observational misinterpretation of major regional feedbacks in the tropical oceans as global ones and provide observational tests for the evaluation of numerical climate models.

The data and methods used in our analysis are described in Section 2. Section 3 examines the influence of high, middle and low clouds on the changes of total cloud and cloud solar forcing. Section 4 analyses the responses of high and low clouds to the interannual variation of SST and the related dynamic processes in order to understand the interannual variations of total cloud. Section 5 explores the influence of cloud variation on SST.

2. Data Sets and Analysis Methods

a. Data Sets

A number of data sets, the International Satellite Cloud Climatology (ISCCP) Stage 2 (C2), National Meteorological Center (NMC) radiosonde, Climate Analysis Center (CAC) SST and European Center for Medium Weather Forecast (ECMWF) analyses (level III) are used together over the tropical oceans to relate the changes of clouds, deep convection, large-scale circulation and SST. The period of this analysis is from July 1983-June 1990. However, the use of ECMWF data is limited to January 1986-December 1990 because of data availability and consistency.

The ISCCP cloud dataset provides a near global distribution of the radiative properties of clouds, atmosphere and surface every three hours (Rossow and Schiffer 1991). These quantities are estimated with the use of a radiative transfer model from the visible (0.55-0.75 μm) and infrared (10.5 -12.5 μm) radiances measured by as many as seven operational satellites. ISCCP C2 is the monthly mean version of the ISCCP cloud dataset. This dataset classifies daytime clouds into seven types according to both cloud optical thickness and cloud top pressure. These are deep convective cloud, cirrostratus, cirrus, nimbostratus, altocumulus, stratus and cumulus clouds. Night-time clouds are more simply classified into low, middle and high according to cloud top pressure derived from IR radiances (Rossow et al. 1991). During daytime, the monthly mean frequency of occurrence, cloud optical thickness and cloud top pressure for each type of cloud are given at each $2.5^\circ \times 2.5^\circ$ latitude and longitude every three hours (UT). The values of these properties in ISCCP C2 are somewhat different from the new version of ISCCP data (D2). However, these systematical differences are largely removed in our analysis of anomalous changes. Thus, our conclusions in this paper should be qualitatively the same as those obtained from the new ISCCP D2. This study uses the averaged daytime cloud radiative properties, representing the averaged daytime behavior of clouds.

The Climate Analysis Center (CAC) SST data (Reynolds 1988) are derived from blended ship-based and satellite measurements for the global ocean with a resolution of $2^\circ \times 2^\circ$

latitude/longitude and a reported accuracy of 1°C. The global surface **zonal** and meridional wind speeds (u_s and v_s) and vertical velocity at 500 mb ($\omega_{500\text{ mb}}$) obtained from **ECMWF** analyses at a $2.5^\circ \times 2.5^\circ$ resolution are used to describe the surface wind divergence and atmospheric vertical **motion**³ for January 1986-December 1990. The standard spatial resolution for our analysis is $2.5'' \times 2.5''$ latitude/longitude corresponding to the original spatial resolution of most of the datasets we use.

b. Methods

i) Classification of cloud type

The seven cloud types reported in the **ISCCP C2** data are simplified into four. These are deep convective cloud, high (cirrus/anvil) clouds (**merged** from cirrostratus and cirrus), middle cloud (merged from nimbostratus and **altocumulus**) and low clouds (merged from stratus and cumulus). High clouds have an optical thickness less than 22.6 (approximately corresponding to 0.7 for **albedo**) and a top above the 440 mb level. Middle clouds have cloud tops located between pressure levels of 440 mb and 680 mb. Low clouds have tops below the 680 mb level, near the typical height of the **tropical** trade cumulus boundary layer top. This cloud-type grouping follows the classic three-cloud type grouping (high, middle and low clouds) used in **previous** studies of cloud climatology (London 1957; Manabe 1969) except that deep convective clouds are distinguished from other high clouds because deep convection is a key factor for linking changes in tropical cloud fields to SST,

How low clouds change is difficult to diagnose because they cannot readily be detected by satellite visible and **infrared** radiometers on the scale of a satellite **pixel**⁴ if they are underneath higher clouds (Rossow and Lacis 1990). Some low clouds under high or middle clouds may not

³ The vertical velocity is analyzed but not shown in the figures in this paper.

⁴ The sizes of satellite pixels in ISCCP data are 5 km to 8 km sampled to 25-30 km spacing,

be seen by satellite radiometers; and the changes of high and middle clouds may create a spurious change in the low cloud field. When the high or middle clouds decrease, satellite radiometers could see low clouds that were previously overshadowed by high or middle clouds, and hence indicate a spurious increase of low clouds. However, in the regions of large-scale subsidence such as the subtropics and eastern tropical Pacific and Atlantic, the detection of low clouds is less problematic since the deep convective and high clouds are relatively infrequent.

Figure 1 shows the fictional contributions of different cloud types to the total cloudiness for the annual mean cloud climatology. In the southeastern Pacific and Atlantic, low clouds contribute more than 80% of the total cloudiness, and in the subtropical eastern Pacific and Atlantic, more than 50% and so should be relatively unaffected by obscuring higher clouds. Changes of high/middle clouds are compared with those of low clouds in the above regions to assure that the changes of low clouds are not largely artifacts of the changes of high/middle clouds (Figure 2). That is, if the changes of low clouds are not anticorrelated with, or larger than, those of high and middle clouds, they cannot be totally caused by the changes of high/middle clouds, and thus should be at least partially real. Figure 2 shows that in (b) the southeastern Pacific and (c) and (d), both north- and southeastern Atlantic, that the changes of low clouds were larger than those of high and middle clouds, and therefore, should correspond largely to real changes of the low clouds. This paper limits its analysis to low clouds in these regions.

ii) The cloud solar effect index

How high, middle and low cloud variations influence solar radiation is estimated by a cloud solar radiation effect index defined as $IS = S_0 A_c (\alpha_c - \alpha_s)$ (cf. Fu et al. 1992), where $S_0 = 339.5 \text{ W m}^{-2}$ is the global annual mean incident solar flux at the top of the atmosphere, A_c the spatial frequency of cloud, $\alpha_s = 6\%$ a typical but somewhat arbitrary value of ocean surface albedo, and α_c the albedo of cloudy sky⁵. IS summarizes the changes of cloud amount and reflectance

⁵ α_c is calculated from ISCCP cloud optical thickness (Rossow et al. 1991).

with one variable to allow a more efficient analysis of the changes of different cloud types. Only these relative changes, not its absolute values, are of interest.

IS differs in several ways from the more commonly used cloud solar forcing (FS_c), (total downward solar flux minus downward solar flux of clear sky) (e.g. Charlock and Ramanathan 1985; Hartmann et al. 1986; Cess and Potter 1987), although it may appear to be superficially similar, except for sign. The change of IS is **solely** caused by the change of cloud amount and reflectance, whereas FS_c depends also on changes in both solar fluxes and clear sky **albedos**. IS is calculated from a cloud cover index and **albedo** inferred from narrow band visible radiances (0.55-0.7 μm), but FS_c is calculated from broad band solar insulation and **albedo** over the full spectrum of 0.2-5.0 μm . More importantly, IS was designed to show changes of cloud properties, whereas FS_c to show changes of solar fluxes associated with clouds at TOA.

iii) Data reconstruction

This analysis focuses on the low frequency **variations, especially interannual**, of clouds and SST and explores their interactions. The tropical cloud field also shows various high frequency variations, for example, synoptic disturbances and the 30-60 days oscillation (Lau and Chan 1988). Lower frequency variations are isolated by applying Empirical Orthogonal Functions (EOFs) to the tropical cloud, SST, wind divergence and vertical velocity fields. Compared to time running mean or temporal **frequency** bandpass filter, EOFs removes both spatial and temporal noise and high frequency variations. Two steps are involved in selecting the modes that will be retained in the reconstructed fields. First, noise modes are removed according to the dominant-variance rule A4 and the time-history rule Q (Preisendorfer et al. 1981). For A4, **eigenvalues** of the data matrix are compared with a **matrix** of **normal**ly distributed random noise of the same size. The criterion in rule Q is determined from the serial correlation function associated with the principal components of the data matrix. Only the EOF modes suggested as **significant** signal modes by both rule A4 and Q are retained. Maximum entropy spectrum analysis is then applied to the time series of each signal mode suggested by rule A4 and rule Q. If the power

spectrum of a given EOF mode peaks at a period longer than three months, it is retained in the data reconstruction. The number of significant EOF modes and variances that are retained in the EOF reconstruction for various variables as listed in Table I are therefore determined by the time scale of variability of a given variable. EOF reconstruction is only **used** to **clarify** the signal, and results are qualitatively the same as those **obtained** from raw data.

To focus on **interannual** variation, the results in Sections 3 and 4 are shown in terms of anomalies of clouds, SST and circulation fields (Figures 1 and 6 excepted). The anomaly of each variable is calculated by subtracting **climatological** monthly means from a particular monthly mean. The **climatological** seasonal cycle is calculated for January 1984-December 1990.

3. How do High, Middle and Low Clouds Influence Total Cloud Variation?

The contribution of each cloud type to the anomalies of total cloudiness is shown in terms of the correlations of the solar radiation **effect** indices of high (**ISHC**), middle (**ISMC**), and low clouds (**ISLC**) with that of total clouds (ISTO) (Figure 3). The correlation between ISHC and ISTO is high and positive (≥ 0.6) in the tropical Indian, western and central Pacific and southwestern Atlantic oceans as indicated by dark shaded areas in Figure 3a. Thus, high clouds dominate the **interannual** variation of total clouds in those regions. These correlations are lower (≤ 0.4) in the eastern tropical oceans where large-scale subsidence usually occurs. ISMC is well correlated to ISTO (Figure 3b) almost everywhere except in the eastern **Pacific** and Atlantic. In sum, the variation of total cloud is dominated by the high and middle clouds over most of the tropical oceans, except for the eastern Pacific and Atlantic. Conversely, ISLC is strongly correlated (≥ 0.6) with ISTO in the eastern Pacific and Atlantic and southwestern Indian oceans as indicated by dark shaded areas in Figure 3c. That is, the variations of low clouds evidently control the variations of total clouds in those areas, as expected since low clouds, especially the stratus and stratocumulus clouds, dominate total cloud population in the eastern tropical oceans (Warren et al. 1988), where the marine trade cumulus boundary layer is well defined. Figure 3 **confirms** the earlier finding of **Ockert-Bell** and Hartmann (1992), that the **total** cloud variation **is** dominated by different cloud types in different geographic areas and dynamic regimes.

4. How do Tropical Clouds Respond to SST Change?

Different dynamic processes control the responses of high and low clouds to the **interannual** variation of SST.

a. Response of high clouds

Local and remote correlations between ISHC and SST are compared over tropical oceans (30°S - 30°N) for July 1983-December 1990 (Figure 4) to explore the relative influence of local SST versus large-scale circulation on variations of high clouds. Positive correlations suggest that **warmer** SSTs increase cloudiness and negative correlations that they decrease cloudiness. The areas of significant negative correlation are shaded by lighter gray and those of significant positive correlation by darker gray. What is a **significant** correlation coefficient is determined from a Student-t test according to the degrees of freedom of the **EOF** reconstructed time series. Figure 4a shows that significant positive correlations between ISHC and local SST were mainly confined to the equatorial central and northeastern Pacific (1°S - 10°N , 160°E - 90°W), where SST anomalies are positive with El Niño, and to the southwestern Pacific where anomalies are negative. In other words, **hi**gh cloudiness increases or decreases in these regions primarily with El Niño cycle increases or decreases of **SSTs**.

Outside of these El Niño areas, the local correlations between ISHC and SST are largely insignificant, suggesting that the changes of high clouds elsewhere are not forced by local SST. In some areas in the eastern equatorial Indian Ocean, the correlations are even negative. A warmer SST increases the buoyancy of the air in the **planetary** boundary layer (**PBL**), so unless this buoyancy is suppressed by other factors, such as subsidence or a stable stratified boundary layer, a warmer SST will promote deep convection and high clouds. **Thus**, the high clouds in the areas of negative correlation cannot be caused by changes of the local SSTs.

The remote correlations between ISHC and SSTN3 (the mean anomalous SSTs of the NINO3 area [5 °S-50N, 150°W-90°W]) relate high clouds to circulation changes (Figure 4b). **SSTN3** indicates the **interannual** change of equatorial SST associated with ENSO. When it is positive, the **zonal** SST gradient decreases in the equatorial Pacific, and the meridional SST gradient increases in the central and eastern **Pacific**. Thus, this remote correlation relates changes of equatorial SST to changes of atmospheric circulation during **ENSO**⁶. Significant positive correlations between **ISHC** and SSTN3 are found in the equatorial central Pacific and north- and southeastern Pacific and Caribbean, showing that high clouds increased in those areas when SST rose in the equatorial eastern Pacific during **El Niño**. Large areas of negative correlations are seen in the Indonesian area, subtropical western and central **Pacific**, and northern equatorial Indian oceans, suggesting that decreases of high clouds in **those** regions are related to warming of the equatorial eastern Pacific.

Changes of surface wind velocity associated with **SSTN3** are indicated by the vectors in Figure 4b. These show how the remote correlation pattern between high clouds and SSTN3 **relates** to **interannual** changes in large-scale circulation. These vectors represent the linear regression coefficients of the **zonal** and meridional surface wind speed versus **SSTN3**, that is the slope of a **least-square** fit line for these two variables; such coefficients are commonly used to quantify the change of one variable as a **linear** function of the another variable (e.g. Lau and Nath 1994). The direction of the arrow in Figure 4b gives changes of surface wind direction, and it indicates how much the surface wind speed changes with **change** of SSTN3. Anomalous surface wind convergence are evidently collocated with the dark shaded areas of high cloud increase during **El Niño**, and anomalous surface wind divergence with the light shaded areas of high cloud decrease. Changes of high **clouds** clearly occur with changes of surface wind divergence except in the eastern equatorial Indian Ocean. In the eastern equatorial Indian Ocean, where

⁶ The correlations among the **interannual** variations of clouds, convection and SST change in the NINO4 area (5°S-5°N, 160°-150°E) are about the same as for NINO3.

observations are sparse, the quality of the data is relatively unreliable and so the determination of anomalous convergence is questionable.

The pattern of high cloud variations in Figure 4b resembles that of typical ENSO-related precipitation anomalies (Ropelewski and Halpert 1987) and outgoing longwave radiation (OLR) anomalies (Rasmussen and Wallace 1983; Lau and Chan 1988). Since the intra-seasonal variation has been removed in this analysis, this pattern is mainly that of interannual variation; Lau and Chan suggest this pattern is also followed by intra-seasonal variations.

The correlations between ISHC and local SSTs shown in Figure 4a are mostly insignificant in the Indonesian area, subtropical western and central Pacific and equatorial eastern Indian oceans so that local SST changes are not the direct cause of the high cloud variations in those regions. The significant correlations among ISHC, SSTN3 and surface wind divergence in Figure 4b imply that the changes of high cloud in those areas mainly follow the large-scale circulation changes associated with ENSO. In the equatorial central and eastern Pacific where El Niño warming occurred, the local and remote correlations are equally strong so that local SST and atmospheric circulation might have a comparable influence on high cloud variations. Alternatively, since the local SST in these areas are also well correlated to SSTN3, the correlations between high clouds and local SST could well be caused by linkages to SSTN3 or vice versa, or both local and remote correlations between high clouds and SST could actually be caused by a third unknown factor. A different analysis is used to obtain more insight into cause-effect relationships in these regions.

Figure 5 presents temporal variations of high cloud, deep convection and SST anomalies in the Pacific for January 1986-June 1988. Figure 5a compares the deep convective cloud (heavy contours), and local SST anomalies (shading) along the equator in the central and eastern Pacific. While strong SST wtig ($\geq 1.5^{\circ}\text{C}$) occurred from December 1986-November 1987, deep convection occurred in the eastern Pacific only in the middle of that period, from February to June 1987. The maximum SST warming occurred to the east of 160°W , but maximum deep convection occurred to the west. This eastward displacement of the maximum SST from the area

of convection indicates a dynamical coupling rather than simply column thermodynamics (cf. Lau and Shen 1988). Furthermore, **maximum** deep convection occurred **in** the eastern Pacific three months **before** the maximum SST anomaly (cf. Fu et al. 1994). Thus the deep convection anomaly **in** the equatorial central **and** eastern Pacific could not have been caused primarily by a local SST anomaly. As expected from Figure 5a, Figure 5b shows that the high cloud variation is also not correlated to local **SST** change over these areas.

Linkages between high clouds and atmospheric circulation changes are further investigated in Figure 6. Figure 6a shows that the occurrence of high clouds is more closely correlated to total SST (**Gadgil et al. 1984; Graham and Barnett 1987**) than are high cloud anomalies to the SST anomalies shown **in Figure 5b**, and that the 28°C **isothermal** extended about 5°-10° in longitude further eastward than the substantial high cloudiness **during** July 1986-January 1987 and July 1987-December 1987. Temporal variations of high clouds and total surface wind convergence are examined in Figure 6b. During the 1987 El Niño, high cloudiness was generally closely correlated to the total surface wind convergence. However, this correlation between high clouds and surface wind convergence does not seem to carry over to seasonal variations in the equatorial eastern Pacific. For example, in the spring of 1986, large-scale high clouds were negligible despite a convergent surface wind field. In conclusion, **Figure 6** shows that the distribution of high clouds is strongly correlated to, but not completely determined by, the surface conditions.

Deep convection occurs only when near surface **air** is potentially more buoyant than is the air above the boundary layer as determined by temperature and humidity. The buoyancy above the atmospheric boundary **layer** is mainly controlled by large-scale vertical motion (**Sarachik 1978; Betts and Ridgway 1988**) and by radiative cooling. This large-scale vertical motion depends on the surface pressure gradient caused by ocean basin-wide surface temperature gradients and land-ocean contrast (e. g. **Bjerknes 1969; Chervin and Druyan 1984, Stone and Chervin 1984; Lindzen and Nigam 1987**) but not the local **SSTs**. On the other hand, the buoyancy of the boundary layer air is strongly influenced by SSTs through their effects on temperature and moisture. Thus the

minimum SSTs required for onset of deep convection depends on the air temperature above the boundary layer.

Changes with ENSO of **vertical** profiles of the equivalent potential temperature (θ_e) and saturation equivalent potential temperature (θ_{es}) are used to estimate the influence of SST and of circulation on convective instability. θ_e is an index of the density change expected from latent heating, The θ_e of a convecting parcel is determined by θ_e at its original altitude and remains constant during the moist convection process. Atmospheric stratification can be measured by θ_{es} . The atmosphere is conditionally unstable for moist convection when $d\theta_{es}/dp > 0$ (lighter below and heavier above) and conditionally stable when $d\theta_{es}/dp < 0$. θ_{es} also indicates the minimum potential temperature that is required for condensation at a given temperature and pressure, Continuous condensation above the atmospheric boundary layer is needed for deep moist convection, Thus, the maximum θ_{es} above the atmospheric boundary layer represents the minimum potential temperature that a convecting **parcel** must have for deep moist convection to occur. Whether or not atmospheric conditions are suitable for deep convection can be determined by checking whether or not θ_e in the atmospheric boundary layer is greater than the **maximum** θ_{es} aloft,

The vertical **profiles** of θ_e and θ_{es} at Tarawa Island (1.4°N, 172.9°E) for May 1987 and 1988 are presented in **Figure 7**, as calculated by the empirical formulae given by Bolton (1980) that incorporate the temperature and humidity dependence of latent heat. They demonstrate the **interannual** variation of atmospheric convective instability in the equatorial central Pacific. In May 1988 (Figure 7a), a non-El Niño month, deep convection and high clouds were infrequent in the equatorial central Pacific (see Figure 6). The θ_{es} profile shows that the atmosphere was then too stable for the air in the **PBL** to convect. Given the values of θ_{es} in the neutral stable layer between 925 mb and 750 mb, it appears that θ_e in the PBL should be greater than 354K for convection to penetrate through this stable layer. However, the mean θ_e of the air rising from the PBL was only about 352K, that is, less than that required for the onset of deep convection. Thus, the main barrier for the occurrence of deep convection was the neutral stable layer between

925 mb and 750 mb. On the other hand, in May 1987 (Figure 7b), an **El Niño** month, deep convection and high clouds were greatly enhanced in the equatorial central **Pacific** (see Figure 6). The θ_{es} profile suggests that the atmosphere was connectively unstable for parcels rising from the PBL; that is, the mean potential of the PBL was about 356K, greater than the **maximum** θ_{es} above 900 mb. Convective instability was enhanced in May 1987 compared to May 1988 because the atmosphere between 900 mb and 750 mb was destabilized ($d\theta_{es}/dp > 0$). This destabilization was strongest between 800 mb and 750 mb, at the top of the tropical convective boundary layer (CBL).

In spite of the 4K warming of θ_e caused by **warmer** SST, convection would not have been much more pronounced at **Tarawa** in May 1987 than in 1988 if the θ_{es} profile between 900 mb to 750 mb had been as stable. If so, θ_{es} between 900 mb and 750 mb would have been 355.5K, or about the same as the mean θ_e of the PBL. On the other hand, if in May 1988, $d\theta_{es}/dp$ between 900 mb and 750 mb were changed to that of May 1987, the atmosphere **would** have been unstable for deep convection without any increase of SSTs. Evidently, relative to normal conditions, destabilization of the atmosphere between 900 mb and 750 mb in the equatorial central Pacific was more important for enhancing deep convection during the 1987 **El Niño**, and the direct effect of local SST warming was less important.

Much of the time, and over most of the tropical oceans, the **atmosphere** is dominated by large-scale subsidence. For such, both observational and theoretical studies suggest that the free atmosphere above the CBL is not locally coupled to the underlying SST (**Betts** 1985; **Betts** and **Albrecht** 1987). By analyzing the Saturation Point, a parameter that can efficiently represent the mixing process and indicates the origins of the air parcels involved in the mixing (**Betts** 1982), **Betts** and **Albrecht** (1987) showed for FIRE (First International Regional Experiment) data that the air at the top of the CBL comes from the overlying atmosphere, rather than from the surface. Thus, the thermodynamic properties at the top of the CBL were directly influenced by the subsidence of the free atmosphere. These results suggest that the **interannual** change of the

conditional instability at **the** top of CBL shown in Figure 7 was mainly caused by the change of large-scale subsidence.

During an El Niño month (May 1987), the vertical velocity at 500 mb of ECMWF analyses (not shown) suggests that anomalous rising vertical motion occurred in the equatorial central Pacific. The smaller differences between θ_e and θ_{es} in May 1987 imply a moister middle and upper troposphere, which is consistent with the above result from the ECMWF analyses. Therefore, changes of large-scale vertical motion apparently force an interannual variation of conditional instability between 900 mb and 750 mb, and **hence** of deep convection and high clouds in that area.

How anomalous subsidence can affect atmospheric convective instability is further examined in Figure 8. θ_e and θ_{es} profiles at Pago Pago Island (14.3°S, 170.7°W) show the **interannual** variation of atmospheric convective instability in the southern central Pacific. In May 1988 (Figure 8a), the atmosphere was **convectively** unstable, consistent with anomalous enhancement of deep convection and high clouds indicated by ISCCPC2 data. By contrast, in May 1987 (Figure 8b), the atmosphere was connectively stable due to both strengthening of the inversion and decreasing of θ_e in PBL. The larger difference between θ_e and θ_{es} and the warmer θ_{es} in the middle troposphere are consistent with the anomalous increase of subsidence suggested by ECMWF analyses. While it is clear that the warmer θ_{es} in the middle troposphere in May 1987 is mainly caused by anomalous enhanced subsidence, it is not so clear what caused the colder θ_e in the PBL.

The CAC SST data suggests that SST was only 0.85°C colder in May 1987 than in May 1988, However, the **radiosonde** data indicate that the air at 1000 mb was about 1.5°C colder and 6% drier in relative humidity in May 1987 than in May 1988, causing about a 6.7K and 3.6K, respective y, reduction of θ_e at 1000 mb in May 1987. Evidently, either the surface temperature change alone or the change of relative humidity in the PBL plus a lapse rate change between 900 mb and 750 mb could stabilize the atmosphere for moisture convection. Since the temperature change in the PBL is probably a direct **result** of SST, whereas the changes of relative

humidity in the PBL and the **lapse** rate between 900 mb and 750 mb are more linked to the dynamic structure of PBL and **free** atmosphere, the changes of SST and the dynamic field evidently were equally important for suppressing deep convection at Pago Pago in the southern central **Pacific** in May 1987. The changes of θ_e and θ_{es} profiles at Midway Island (28.2°N, 177.4°E) in the northern central Pacific between **El Niño** and non-El Niño periods were similar to those in the southern central Pacific indicated in Figure 8.

Figures 4 through 8 show how changes of large-scale circulation can link variations of high clouds to **interannual** changes of SSTs. Anomalous large-scale rising motion enhanced both deep convection and high clouds by destabilizing the **atmosphere** between 900 mb and 750 mb in the equatorial central and eastern Pacific during the 1987 **El Niño**. The direct effects of local SST were less important than **was** this change of atmospheric vertical motion. Outside of the equatorial warming areas, both surface conditions and anomalous sinking motion suppressed deep convection and high cloud by **reducing** the buoyancy of PBL air and stabilizing the atmosphere between 900 mb and 750 mb. These results demonstrate that the apparent lag correlation found . by **Arking** and **Ziskin** (1994) between clouds and SST in the equatorial Pacific is actually caused by a change in the large-scale **circulation** responding to the change of SST gradient. However, the large-scale interannual variation of SSTs, and especially the SST gradient, is important for such atmospheric circulation changes, and hence, indirectly, for the **interannual** variation of high clouds. This point has been **more** explicitly illustrated by Del Genio et al. (1995) using the atmospheric general circulation model experiments. Through a pair of experiments, one with an elevated but unchanged SST gradient and the other with a changed SST gradient, they demonstrate that the change of SST gradient is **more** important than a change of SST in determining the cloud change.

b. Response of low clouds

The large-scale oceanic low clouds **in** the eastern Pacific and Atlantic are mainly trade cumulus boundary layer (**TCBL**) clouds that prevail in areas of subsidence. Above the TCBL, subsidence tends to warm and dry the atmosphere adiabatically, whereas within **it**, the atmosphere is cooled and moistened by fluxes from the underlying ocean. Consequently, an inversion layer forms at the top of TCBL and caps the clouds within the **TCBL**. The formation of TCBL cloud **reinforces** the inversion by evaporation and radiative cooling at the bottom of the inversion layer. Thus both SSTs and subsidence can influence these low clouds (**Betts and Ridgway** 1989). Previous observational studies suggest that low clouds are sensitive to changes in the stability of the lower troposphere, and to the **advection** that is associated with either SST gradient (**Deser et al.** 1993), or to the SST upwind of the low clouds (Klein et al. 1995), but not to SSTs (Klein and Hartmann 1993).

This section examines the relationships of SST and circulation to the **interannual** variation of low clouds. Figure 9, like Figure 4 for ISHC, compares the local correlation between ISLC and SST and the remote correlation between ISLC in the eastern **Pacific** and Atlantic oceans and SSTN3 where low clouds dominate the total cloud population and high clouds are datively infrequent (Figure 1). Negative local correlation between **ISLC** and SST is found in both regions (Figure 9a). In the equatorial eastern Atlantic, ISLC variations are **uncorrelated** to ISHC, and thus not an artifact. **Interannual** changes of low clouds in the eastern Pacific have been studied by other investigators (see review in Klein et al. 1995), but the **remote** correlation between low clouds in the equatorial eastern Atlantic and **SSTN3** has not been **previously** examined. These changes in low cloudiness appear to correlate with both local SST and SSTN3.

Low clouds can be affected by many factors such as cold-air advection, shear-generated turbulence and cloud-top **entrainment** instability (**CTEI**). In the subtropical oceanic areas, it is generally believed that CTEI (Lilly 1968; Randall 1980; **Deardorff** 1980; **MacVean** and Mason

1990; Kuo and Schubert 1988; Siems et al. 1990; Siems and Bretherton 1992) determines variations of low clouds, although the criterion for CTEI to occur and the physical processes involved in determining CTEI are not yet conclusive. There are three criteria for CTEI: the strength of buoyancy reversal must exceed a threshold; there must exist entraining eddies of Richardson number one or less; and the Reynolds number of the entraining eddies must exceed the criteria for turbulence. The last two conditions are generally met with stratocumulus clouds, so, it is the buoyancy criterion and hence strength of inversion that is critical for the CTEI and so for the amount of low clouds. The strength of inversion can be affected by atmospheric vertical motion and by SSTs. Examining θ_e and θ_{es} profiles will help to distinguish which of these effects is most important for the structure of an inversion.

The θ_e and θ_{es} profiles at St. Helena Island (16°S, 5.7°W) in May 1988 and 1987 are shown in Figure 10 to illustrate the influences of local SST change and of vertical motion on the interannual variation of low cloud in the equatorial southeastern Atlantic. In May 1988 (Figure 10a), the inversion was relatively weak ($d\theta_{es}/dp \approx -0.1$ K/rob) and the air above the CBL was drier. That is, there was a bigger difference between θ_e and θ_{es} at the top of inversion layer (750 rob). According to the CTEI theory, a weak enough inversion allows unstable vertical mixing between dry air above the CBL and the cloudy air inside the CBL. The drier air above the CBL would enhance the evaporation of the cloudy air in the CBL as it sinks. Thus, both the temperature inversion and the humidity profile shown in Figure 10a would promote the entrainment of dry air at the cloud top and the breaking of the low clouds. The anomalous decrease of low clouds in May 1988 suggested by satellite observation is consistent with this interpretation. In May 1987, at the time of the El Niño (Figure 10h), the inversion became much stronger ($d\theta_{es}/dp \approx -0.34$ K/rob) and the air above the CBL was more moist than in May 1988. Both these conditions would suppress dry air entrainment at the cloud top and thus promote the increase of low cloud amount. Satellite observations indicate the occurrence of excess low clouds at that time.

How vertical motion compares with local SSTs in influencing the inversion can be inferred from the θ_e and θ_{es} profiles in Figures 10a and b. Below the bottom of the inversion (around 900 mb), θ_e and θ_{es} profiles were very similar in May 1987 and 1988 (CBL was slightly drier in May 1987); that is, there was little **interannual** variation of temperature and humidity structure below the inversion layer. The change of the conditional instability was mainly caused by a vertical shift in the top of the inversion layer. Since the air at the top of CBL comes from above, the lower inversion in Figure 10b for May 1987 must have been caused by a stronger subsidence, pushing the inversion layer to a lower altitude. The stronger subsidence was probably forced by the enhancement of deep convection in the equatorial eastern Pacific since (Figure 9) the ISLC in the equatorial southeastern Atlantic was **remotely correlated** to SSTN3.

c. Response of the total cloud

The **interannual** variations of total clouds is the net result of the changes in the **interannual** variations of high and low clouds as just examined. Figure 11 shows the linear regressions of ISTO, ISHC and ISLC with SSTN3 for July 1983-December 1990. These plots show the cloud changes associated with ENSO. The linear regression coefficients are not only determined by the magnitude of the cloud changes, but also by the correlation between the cloud changes and SSTN3 (equatorial eastern Pacific). High cloudiness is more strongly influenced by the changes of large-scale cumulation associated with ENSO, so it is better correlated to SSTN3. Thus, the regression coefficients are generally larger than those for low clouds. The changes of low clouds are less affected by ENSO related cumulation changes, so their correlation is relatively weak even though the magnitude of low cloud changes are not necessarily small. The sum of the regression coefficients of ISHC, ISMC and ISLC is not necessarily equal to that of total clouds.

Figure 11a represents the change of total clouds over tropical oceans associated with a 1°C warming of SSTN3. The only regression coefficients that are plotted are those above the 95% significant level. A positive/negative coefficient indicates an increase/decrease of total

clouds and solar reflection associated with the 1°C warming of SSTN3. In response to a 1°C warming of SSTN3, total clouds increased over a large area in the equatorial central Pacific and a smaller region in the southeastern Pacific. As inferred from the definition of ISTO, these additional total clouds would reflect up to $14\text{--}18 \text{ W m}^{-2}$ more solar radiation in the equatorial central Pacific, and Up to $2\text{--}6 \text{ W m}^{-2}$ more in the southeastern Pacific. Furthermore, decreases of total clouds in the western and subtropical central Pacific; the Indonesian area, the northeast Indian Ocean and some areas in the equatorial eastern and southeastern Pacific all would cause decreases of solar radiation in the range of $2\text{--}6 \text{ W m}^{-2}$. The large-scale variation of high clouds (Figure 1 lb) was similar to that of the total clouds, in the western and central Pacific and in the northeastern Indian Ocean. For each 1°C warming of SSTN3, increasing high clouds would reduce downward solar radiation by up to $14\text{--}18 \text{ W m}^{-2}$ in the equatorial central Pacific, by about $2\text{--}6 \text{ W m}^{-2}$ in the north equatorial eastern Pacific, and by about $2\text{--}6 \text{ W m}^{-2}$ in the southeastern Pacific, the equatorial and northern subtropical Atlantic oceans. Likewise, decreasing high clouds in the western and subtropical central Pacific and northeastern Indian oceans would cause about $2\text{--}6 \text{ W m}^{-2}$ less solar reflection. Evidently, changes of high clouds are the most important contribution to the changes of total clouds, and to reflection of solar radiation in response to ENSO.

The large-scale change of low clouds (Figure 1 lc) in the subtropical eastern Pacific and eastern Atlantic was mostly opposite to that of high clouds in the subtropical eastern Pacific and eastern Atlantic. Decreased low clouds would increase downward solar radiation by about $9\text{--}11 \text{ W m}^{-2}$ in the subtropical eastern Pacific, and by about 3 W m^{-2} in the northern Atlantic and subtropical southern Atlantic ocean. An increase of low clouds would decrease downward solar radiation in the equatorial and southern tropical Atlantic by about 3 W m^{-2} . Because of this opposite response of clouds to the El Niño, large-scale, low-frequency change of total clouds was near zero in some areas of the equatorial and northeastern Pacific. In general, low clouds variation had an even more important effect on total clouds than did high clouds variation in the

southeastern Pacific and Atlantic (Figure **3c**). Therefore, studying the behavior of each cloud type is necessary for a **more** precise explanation of the changes of total clouds and cloud solar forcing.

5. How Does Cloud Variation Influence SSTS?

Clouds influence SSTS, not only by changing the magnitude of surface solar flux itself, but also by competing **with** other terms **in** the ocean heat budget equation. Although clouds can substantially modulate surface solar fluxes **in** the equatorial **Pacific** during El **Niños**, how this might affect SSTS is still debatable. Numerical models with prescribed seasonal SSTS have **successfully** reproduced the **interannual** variation of SSTS to the **first** order approximation in the equatorial Pacific without such feedback (e.g. **Zebiak** and Cane 1987). A number of observational results also show only a weak contemporaneous correlation between cloud solar radiation changes and SSTS on **interannual** scales (Meyers et al. 1986; Chertock et al. 1990; Liu et al. 1994). Other studies suggest that clouds are a major factor in determining the SSTS, including **their** interannual changes (e.g. **Ramanathan** and Collins 1991). **Waliser** and Graham (1993) pointed out that the change of SST tendency would not be in phase with that of SSTS even if the changes of SSTS were dominated by clouds. Thus a weak contemporaneous correlation between the changes of clouds and SSTS does not necessarily imply a weak effect of clouds on SSTS. Consequently, a coherence analysis is used to examine the correlation as well as phase relationship between clouds and SSTS. This analysis more vigorously tests the cloud effect on SSTS than would a contemporaneous correlation.

The anomalous heat balance of the ocean mixed layer is written:

$$\rho C_p H (dT_s/dt) = Q_s + Q + Q_o \quad (1)$$

where ρ is the ocean water density, C_p the specific heat at constant pressure, H the depth of ocean mixed layer, Q the combined effect of anomalous latent, longwave and sensible heat fluxes, and Q_o the effect of anomalous **advection** and vertical mixing, and Q_s the solar forcing by cloud variation. Because the time scale of the ocean mixed layer response **to** the surface heating change is much faster than one month, the contemporaneous correlation between monthly Q_s and dT_s/dt *will be* strong if Q and Q_o are negligible and H is invariant. A coherence analysis explores

whether first, Q and Q_o introduce significant time lag in the correlation, and second, whether different cloud types produce different **correlations**.

Because SST anomalies are small compared to SSTs in the tropical oceans, we assume $Q \approx -F(U, RH, \delta T)T_s$, where U is surface wind speed, RH is relative humidity and δT is air-sea temperature difference at the ocean surface. Because existing observations do not show **any** direct relationships between RH and T_s or δT and T_s , we assume they are not functions of T_s . We also assume, for simplicity, that U is not a function of T_s even though the wind divergence could be related to the gradient of T_s under certain conditions (Lindzen and Nigam 1987). Although Q_o can be important, we drop this term to simplify our analysis and concentrate on the surface flux. This will not affect our evaluation as to the importance of clouds. If clouds are the most important factor, Q_o is relatively unimportant and we should still **find** a strong coherence between clouds and SSTs. If the coherence **between** clouds and SSTs is weak, adding Q_o would further weaken the coherence. With Q dropped, Equation (1) is written:

$$a \frac{dT_s}{dt} + F(U, RH, \delta T)T_s = Q_s \quad (2)$$

where $a = (\rho C_p H)^{-1}$. Since the oscillating time series of ISTO is close to sinusoidal, Equation (2) shows that if the FT_s term is relatively small, the first and last terms will be in near balance and so dT_s/dt in phase with Q_s . On the other hand, if the FT_s term largely cancels the solar forcing, T_s will be in phase with Q_s and dT_s/dt will lead- Q_s (lag ISTO) by nearly $\pi/2$. More generally, assuming $Q_s = C \exp(i\omega t)$,

$$\frac{dT_s}{dt} = \frac{(Q_s / a) \exp(i\psi)}{(\omega^2 + (F/a)^2)^{1/2}} \quad (3)$$

where $\psi = \pi/2 - \arctan(\omega a / F)$ showing explicitly that the phase of the tendency depends on the ratio of ocean thermal inertia a to the cloud dampening factor F , and suggesting a lag correlation between dT_s/dt and Q_s (cf. Waliser and Graham 1993). Thus an examination of the spatial

distributions of temporal lag correlation between cloud and SST tendency variations clarify how important cloud variation is for SST change.

The magnitude of coherence describes the consistency of the **relative** phase angle of the same frequency between two **time** series, and can be interpreted as similar to the value of the correlation coefficient (Tick 1967; Halpern 1973). The phase of **coherence** indicates the relative phase angle difference of the same frequency. We apply a coherence analysis to the time series of ISTO, the dominant factor of Q_s , and dT_s/dt to investigate the phase relationships between clouds and SST tendency variations in tropical oceans. The hypothesis that cloud fluctuations determine temperature variations would be confirmed by a great coherence magnitude and Q_s , represented by -ISTO leading dT_s/dt by 0° to 90° .

To focus on the low **frequency** variabilities, we analyze the coherence for the frequency window whose periods range from 7.5 to 45 months. Figure 12 shows the geographic distributions of **coherence** (Figure 12a) and phase (Figure 12b) between ISTO and dT_s/dt in the global tropical oceans for the period July 1983-December 1990. In general, the coherence in the equatorial Pacific is not particularly high, although cloud variation is at a maximum in that area. More importantly, Q_s (-ISTO) lags dT_s/dt by about $\pi/2$ to $3\pi/4$ in the equatorial Pacific (Figure 12b). This implies that Q_s lags T_s about π to $5\pi/4$. Thus, Q_s is nearly out-of-phase with T_s in the equatorial **Pacific**. This phase difference is consistent with the positive contemporaneous correlation between T_s and ISTO in the equatorial Pacific (Figure 4a). Both suggest that T_s increases as Q_s decreases, caused by an increase of ISTO in the equatorial Pacific. Thus, the changes of SST are not forced by clouds in this region. Outside of the equatorial Pacific and Atlantic, Q_s leads dT_s/dt in some areas. Thus, clouds might affect the changes of SST, although the cloud anomalies themselves were relatively small compared to those in the equatorial Pacific.

This result indicates that the competition between solar radiation change caused by cloud variation and other factors such as latent and sensible heat fluxes, ocean dynamics and mixing is important in determining the effect of cloud variations on **interannual** variations of **SSTs**.

Different types of clouds in different geographic areas influence SST. We have applied a similar coherence analysis to **ISHC**, **ISMC** and **ISLC**, **respectively**, and dT_s/dt . *Only in* the northwestern subtropical Pacific may **ISHC** affect dT_s/dt . *In* the southern subtropical Pacific and eastern **Pacific**, the coherence between **ISLC** and dT_s/dt suggests that these variations of low cloud may have an important effect on SST. The importance of looking at the behavior of different cloud types in studying the interaction between tropical clouds and SST is again emphasized. Figure 12 indicates that the cloud changes associated with El **Niño** do not control the interannual variation of tropical SST. These results are consistent with the earlier contemporaneous correlation analyses of Liu and **Gautier** (1990) and Liu et al. (1994), and **further** suggest that changes of surface solar flux are not important for determining the sign of **interannual** variation of SST in most tropical oceans.

6. Summary and Conclusions

The large-scale **interannual** variations over the tropical oceans of high, middle, low and deep convective clouds, and surface wind divergence **and** SST, are investigated with the use of **ISCCP C2**, NMC **radiosonde** and CAC SST data sets, and **ECMWF** analyses for **July** 1983-December 1990. What controls cloud response to **ENSO-related** SSTs perturbations is diagnosed in terms of links between the different cloud types, atmospheric thermodynamic structure, cumulation and SST. Tropical clouds are shown to respond to **interannual** variation of SST through different processes in different dynamic regimes. In particular, the sign and strength of the total cloud response to the SST perturbation over much of the tropical oceans is mainly determined by that of high clouds, but low clouds dominate total cloudiness in some areas in the eastern **Pacific** and Atlantic oceans. Large-scale vertical motions are important in controlling the response of tropical clouds to changes of **SSTs**. Cloud variations affect SST not only by their variation, but also by the competition between solar radiation change caused by clouds and other factors in the heat balance of the tropical ocean mixed layer.

The variation of total cloudiness is dominated by high and middle clouds in the western and central tropical oceans, as was assumed **in** previous studies. Changes **in** large-scale vertical motions, resulting from changes of large-scale gradients of **SSTs**, contribute to the change of convective instability in tropical oceans. Destabilization of the atmosphere between 900 mb and 750 mb enhances deep convection in the equatorial central Pacific during the 1987 El **Niño**. The direct local effect of SST variation alone would not have introduced convective instability. In the subtropical Pacific and the equatorial and southern Atlantic, both stabilization of the atmosphere between 900 mb and 750 mb and decreasing θ_e in PBL. reduce deep convection. The direct local effect of SST and the effect of vertical motion are equally important

In the subtropical eastern Pacific and the west coasts of Africa and Australia, low cloud variations make important contributions to the total cloud variation. The increase of low cloud is consistent with the strengthening of the inversion in the equatorial eastern Atlantic as a result of

greater of subsidence during the 1987 El Niño. Local SST change could not have strengthened its inversion, although the variation of low clouds appears to correlate with the variation of local SST in that region.

The coherence between cloud solar radiation indices and SST variations is below the level of statistical significant in most of the tropical oceanic areas, especially in the tropical **Pacific**. Cloud variations do not control the SST tendency in the. equatorial central Pacific, despite the very strong changes of clouds and surface solar radiation (**Liu et al. 1994**) that have been observed in that region during the 1987 El Niño. In some subtropical Pacific areas, the coherence between cloud SST tendency is stronger, although the magnitude of cloud changes are not as strong as those in the equatorial central Pacific. A possible local influence of cloud variation on SST tendency variation is found only in the subtropical Pacific, northern Atlantic and some areas of the Indian ocean indicating that in those regions, the competition between cloud variation and other factors, such as ocean dynamics and evaporation, are important for determining SST. In most areas where cloud variations- might have -important effects on SSTs, the changes of low clouds are also important. Thus, understanding the behavior of different type of clouds is important for assessing the impact of tropical clouds on SST.

Acknowledgments: This research was performed at the Jet Propulsion Laboratory (JPL), California Institute of Technology, under contract with the National Aeronautics and Space Administration (NASA) and completed at the University of Arizona (UA). It was supported by Interdisciplinary Science Investigations of Earth Observing System at JPL and UA, under NASA grants U.P.N. 428-81-22 and 429-81-22 and by the Global Change Data Analysis Branch of NASA. We are grateful to William Rossow, Anthony Del Genio and Chidoug Zhang, and for their invaluable comments on the manuscript. We also thank David Neelin, Michael Ghil, Jiayan Yang and Duane **Waliser** for constructive discussion, K.M. Lau and an anonymous reviewer for

their thorough comments, and **Wenqing** Tang for her help in getting the radiosonde data and ECMWF analysis.

References:

- Arking, A. and D. Ziskin, 1994: Relationship between clouds and sea surface temperature in the western tropical Pacific. *J. Climate*, 7, 988-1000.
- Betts, A. K., 1982: Saturation Point analysis of moist convective overturning. *J. Atmos. Sci.*, 39, 1484-1505.
- Betts, A. K., 1985: Mixing line analysis of clouds and cloudy boundary layers. *J. Atmos. Sci.*, 42, 2751-2763.
- Betts, A.K. and B.A. Albrecht, 1987: Conserved variable analysis of boundary layer thermodynamic structure over the tropical oceans. *J. Atmos. Sci.*, 44, 83-99.
- Betts, A.K. and W. Ridgway, 1988: Coupling of the radiative, convective and surface fluxes over the equatorial Pacific. *J. Atmos. Sci.*, 45, 522-536.
- Betts, A.K. and W. Ridgway, 1989: Climatic equilibrium of the atmospheric convection boundary layer over a tropical ocean, *J. Atmos. Sci.*, 46, 2621-2641.
- Bjerknes, J., 1969: Atmospheric teleconnections from the equatorial Pacific. *Mon. Wea. Rev.*, 97, 163-172.
- Bolton, D., 1980: The computation of equivalent potential temperature *Mon. Wea. Rev.*, 108, 1046-1053.
- Cess, R. D., G.L. Potter, J.P. Blanchet, G.J. Boer, A.D. DelGenio, M. Deque, V. Dymnikov, V. Galin, W.L. Gates, S.J. Ghan, J.T. Kiehl, A. Lacis, H. LeTreut, Z.-X. Li, X.-Z. Liang, B.J. McAvaney, V.P. Meleshko, J.F.B. Mitchell, J.-J. Morcrette, D.A. Randall, L. Rikus, E. Roeckner, J.F. Royer, U. Schlese, D.A. Sheinin, A. Slingo, A.P. Sokolov, K.E. Taylor, W.M. Washington, R.T. Wetherald, I. Yagai and M.-H. Zhang, 1990: Intercomparison and

- interpretation of climate feedback processes in 19 atmospheric general circulation models. *J. Geophys. Res.*, 95, 16601-16615.
- Cess, R.D. and G.L. Potter, 1987: Exploratory studies of cloud radiative forcing with a general circulation model. *Tellus*, 39A, 460-473.
- Charlock, T.P. and V. Ramanathan, 1985: The albedo field and cloud radiative forcing produced by a general circulation model with internally generated cloud optics, *J. Atmos. Sci.*, 42, 1408-1429.
- Chertock, B., R. Frouin, and R.C.J. Somerville, 1990: Global monitoring of net solar irradiance at the ocean surface: climatological variability and the 1982-1983 El Niño. *J. Climate*, 4, 639-650.
- Chervin, R.M. and L.M. Druyan, 1984: The influence of ocean surface temperature gradient and continentality on the Walker Circulation. Part I: Prescribed tropical changes. *Mon. Wea. Rev.*, 112, 1510-1523.
- Deardorff, J.W., 1980: Cloud top entrainment instability. *J. Atmos. Sci.*, 37, 131-147.
- DelGenio, A. D., M.S. Yao, W. Kovari, and K.K.- W. Lo, 1995: A prognostic water parametrization for global climate models. Submitted to *J. Clim.*
- Deser, C., J. J. Bates, and S. Wahl, 1993: The influence of sea surface temperature gradients on stratiform cloudiness along the equatorial front in the Pacific ocean, *J. Climate*, 6, 1172-1180.
- Fu, R., A.D. Del Genie, W.B. Rossow, and W.T. Liu, 1992: Cirrus-cloud thermostat for tropical sea surface temperatures tested using satellite data. *Nature*, 358, 394-397.
- Fu, R., A.D. Del Genie, and W.B. Rossow, 1994: Influence of ocean surface conditions on atmospheric vertical thermodynamic structure and deep convection. *J. Climate*, 7, 1092-1108.

- Gadgil, S. P., P.V. Joseph, and N.V. Joshi, 1984: Ocean-atmosphere coupling over monsoon regions. *Nature*, **312**, 141-143.
- Graham, N.E and T.P. Barnett, 1987: Observations of sea surface temperature and convection over tropical oceans. *Science*, **238**, 657-659.
- Halpern, D., 1973: On the estimation of a complex-valued coherency function using a discrete fourier transform. *Proceeding of the 3rd. Conference on Probability and Statistics in Atmospheric Sciences*, Boulder, Colorado, June 1973, 157-164.
- Hartmann, D. L., V. Ramanathan, A. Berroir, and G.E. Hunt, 1986: Earth Radiation Budget data and climate research. *Rev. Geophys.*, **24**, 439-468.
- Hartmann, D.L. and Michelson, M. L., 1993: Large-scale effects on the regulation of tropical sea surface temperature. *J. Climate*, **6**, 2049-2062.
- Heymsfield, A.J. and L.M. Miloshevich, 1991: Limit to greenhouse warming? *Nature*, **351**, 14-15.
- Klein, S. A. and D. L. Hartmann, 1993: The seasonal cycle of low stratiform clouds. *J. Climate*, **6**, 1587-1606.
- Klein, S.A., D.L. Hartmann, and J.R. Norns, 1995: On the relationship among low cloud structure, sea surface temperature, and atmospheric circulation, Submitted to *J. Climate*.
- Kuo, H. and W. H. Schubert, 1988: Stability of cloud-topped boundary layers. *Quart. J. Roy. Meteor. Soc.*, **114**, 887-916.
- Lau, N.C. and M.J. Nath, 1994: A modeling study of the relative roles of tropical and extratropical SST anomalies in the variability of the global atmospheric-ocean system. *J. Climate*, **7**, 1184-1207.
- Lau, K.M. and P.H. Chan, 1988: Intraseasonal and interannual variations of tropical convection: A possible link between the 40-50 day oscillation and ENSO? *J. Atmos. Sci.*, **45**, 506-521.

- Lau, K. M., **C.H. Sui**, M.D. Chou and **W.K. Tao**, 1994: An inquiry into the cirrus-cloud thermostat effect for tropical sea surface temperature. *Geophy. Res. Let.*, **21**, 1157-1164.
- Lau, **K.M.** and S. **Shen**, 1988: On the dynamics of **intraseasonal** oscillation and ENSO. *J. Atmos. Sci.*, **45**, 1781-1797
- Lilly, D. K., 1968: Models of cloud-topped mixed layers under a strong inversion. *Quart. J. Roy, Meteor. Soc.*, **94**, 292-309.
- Lindzen, R.S.** and S. Nigarn, 1987: On the role of sea surface temperature gradients in forcing low-level winds and convergence in the tropics. *J. Atmos. Sci.*, **44**, 2418-2436.
- Liu, **T.W.** and C. **Gautier**, 1990: Thermal forcing on the tropical Pacific from **satellite** data. *J. Geophys. Res.*, **95**, 13,209-13,217.
- Liu, T.W., **A.Z. Zhang**, and **J.K.B. Bishop**, 1994: Evaporation and solar **irradiance** as regulators of sea surface temperature in annual and **interannual** changes. *J. Geophys. Res.*, **99**, 12,623-12,637.
- London, J., 1957: A study of the atmospheric heat balance. *Rep. Contract AF19 (122)-165*, College of Engineering, **New York University** [ASTLA No. 117227].
- Manabe, S., 1969: Climate and ocean circulation. Part I: The atmospheric circulation and the hydrology of the earth's surface. *Mon. Wea. Rev.*, **91**, 739-774.
- MacVean, M. K., and **P.J. Mason**, 1990: Cloud-top entrainment instability through small-scale mixing and its **parameterization** in numerical models. *J. Atmos. Sci.*, **47**, 1012-1030.
- Meyers, G., **J.R. Donguy**, and **R.K. Reed**, 1986: Evaporative cooling of the western equatorial Pacific ocean by anomalous winds. *Nature*, **323**, 523-526.
- Ockert-Bell, M.E.** and **D.L. Hartmann**, 1992: The effect of cloud type on earth's energy balance: results for selected regions. *J. Climate*, **5**, 1157-1170

- Pierrehumbert, R.T., 1995: Thermostats, radiator fins, and the local runaway greenhouse. *J. Atmos. Sci.*, in press.
- Preisendorfer, R. W., W.Z. Francis, and T.P. Barnett, 1981: Foundations of principal component selection rules. *SIO reference series 81-4*, Scripps Institution of Oceanography, University of California, May, 1981.
- Ramanathan, V. and W. Collins, 1991: Thermodynamic regulation of ocean warming by cirrus clouds deduced from observations of the 1987 El Niño. *Nature*, **351**, 27-32.
- Randall, D. A., 1980: Conditional instability of the first kind upside-down. *J. Atmos. Sci.*, **37**, 125-130.
- Rasmussen, E. M., and J.M Wallace, 1983: Meteorological aspects of the El Niño/Southern Oscillation. *Science*, **222**, 1195-1202.
- Reynolds, R.W., 1988: A real-time global sea surface temperature analysis. *J. Climate*, **1**, 75-86.
- Ropelewski, C.F. and M.S. Halpert, 1987: Global and regional scale precipitation patterns associated with the El Niño/Southern Oscillation. *Mon. Wea. Rev.*, **115**, 1606-1626.
- Rossow, W. B., and A.A. Lacis, 1990: Global, seasonal cloud variations from satellite radiance measurements. Part II: cloud properties and radiative effects. *J. Climate*, **3**, 1204-1253.
- Rossow, W. B., L.C. Garder, P.J. Lu, and A. Walker, 1991: International Satellite Cloud Project (ISCCP) documentation of cloud data. In, *WMO/TD No. 266, World Climate Research Program (ICSU/WMO)*, 75pp, plus three appendices.
- Rossow, W.B. and R.A. Schiffer, 1991: ISCCP cloud data products. *Bull. Amer. Meteor. Soc.*, **72**, 1-20.
- Sarachik, E. S., 1978: Tropical sea surface temperature: an interactive one-dimensional atmosphere ocean model. *Dyn. Atmos. Oceans*, **2**, 455-469.

- Seager, R. and M.B. Blumenthal**, 1995: Modeling tropical Pacific sea surface temperature with satellite-derived solar radiative forcing. *J. Clim.*, in press.
- Senior, C.A. and J.F.B. Mitchell**, 1993: Carbon dioxide and climate: The impact of cloud parametrization. *J. Clim.*, **6**,393-418.
- Siems, S. T., R.E. Bretherton, M.B. Baker, S.S. Shy, and P.K. Smolarkiewicz**, 1990: Buoyancy reversal and cloud-top entrainment instability. *Q. J. Roy. Meteor. Soc.*, **116**, 705-739.
- Siems, S.T., and C.S. Bretherton**, 1992: A numerical investigation of cloud-top entrainment instability and related experiments. *Q. J. Roy. Meteor. Soc.*, **118**, 787-818.
- Stephens, G. and T. Slingo**, 1992: An air-conditioned greenhouse. *Nature*, 358,394-397.
- Stone, P.H. and R.M. Chervin**, 1984: The influence of ocean surface temperature gradient and continentality on the Walker Circulation. Part II: Prescribed global changes. *Mon. Wea. Rev.*, **112**, 1524-1534.
- Tick, L. J.**, 1967: Estimation of coherency. *Spectral analysis of time series*, 133-152, Harris, editor, John Wiley, 319 pp.
- Walker, D.E. and N.E. Graham**, 1993: Convective cloud systems and warm-pool SSTs: coupled interactions and self-regulation. *J. Geophys. Res.*, **98**, 12,881-12,893.
- Wallace, J. M.**, 1992: Effect of deep convection on the regulation of tropical sea surface temperature. *Nature*, **357**,230-231.
- Warren, S. G., C.J. Hahn, J. London, R.M. Chervin and R.L. Jenne**, 1988: Global distribution of total cloud cover and cloud type amounts over the ocean. *NCAR Technics/ Notes*, **NCAR/TN-317+STR**, pp42.
- Washington, W. and G. Meehl**, 1993: Greenhouse sensitivity experiments with penetrative cumulus convection and tropical cirrus albedo effects. *Clim. Dynam.*, **8**, 211-223.

Zebiak, S.E. and M.A. Cane, 1987: A model El Niño-Southern Oscillation. *Mon. Wea. Rev.*, **115**, 2262-2278.

Figure Captions

Figure 1: (a) **Climatological** annual mean fractional contribution of total ISHC to total ISTO over the global tropical oceans for **January** 1983-December 1990. **The** contour interval is 20%. (b) As in (a) but for total **ISMC**. (c) As in (a) but for total **ISLC**.

Figure 2: Time series of anomalous cloud amount index of the sum of the deep convective, high and middle clouds and the cloud amount index of the low clouds at (a) **21.25°N, 121.25°W**; (b) **21.25°S, 101.25°W**; (c) **18.75°N, 28.75°W**; (d) **11.25°S, 8.75°W**.

Figure 3: (a) The maps of contemporaneous correlation coefficients between **ISHC** and ISTO over the global tropical oceans for July 1983-December 1990. Solid contours represent positive correlation and dashed contours represent negative correlation. Contours start from 0.6 and increase by an interval of 0.2. The areas where the absolute values of correlation coefficient are greater than 0.6 are shaded. (b) As in (a) but for the contemporaneous correlation between **ISMC** and ISTO. (c) As in (a) but for the contemporaneous correlation between **ISLC** and ISTO. The critical correlation coefficient for a 95% confidence level is 0.28 for all plots.

Figure 4: (a) Map of the correlation coefficients between **ISHC** and local SST anomalies reconstructed **from** EOFs over the global tropical oceans for July 1983-December 1990. Solid contours show a positive correlation and the dashed contours a negative correlation. Contours start from **±0.4** and **increase** or decrease by an interval of 0.2. The critical correlation coefficient at a 95% confidence level is **±0.62**. The areas with significant **local** correlation coefficients are shaded. (b) The contours represent the remote correlation coefficient between EOF reconstructed ISTO over the global tropical oceans on a **2.5°×2.5° latitude/longitude** map cell and SSTN3 for July 1983-December 1988. The contours and shadings **are** defined in the same way as in (a). The vector field **represents** the linear **regression** coefficient between the **anomalies** of global surface

wind velocity and SSTN3. The arrow indicates the direction of the surface wind anomalies and the length indicates the magnitude of the surface wind anomalies obtained from the linear regression. The scale of the vector is indicated on the low-right side of the figure.

Figure 5: (a) **Hovmöller** diagram of the anomalous frequency of deep convective cloud and SST at equator (1.25°N) in the central and eastern Pacific (170°E - 90°W) for January 1986-July 1988. The thick contours represent the anomalies of deep convective cloud frequency, starting from ± 2.5 and increasing or decreasing by an interval of 5. The thin contours and shadings represent SST anomalies, starting from $\pm 1^{\circ}\text{C}$ and increasing or decreasing by an interval of 1°C . The solid contours show positive anomalies and the dashed contours negative anomalies. Dark gray shading indicates SST anomalies greater than 1°C , light gray shading SST anomalies less than 1°C . (b) As in (a) but the thick contours are for **ISHC**, starting from $\pm 5 \text{ W m}^{-2}$ and increasing or decreasing by an interval of 10 W m^{-2} .

Figure 6: (a) **Hovmöller diagram** of the total **ISHC** and SST at the equator (1.25°N) and in the central and eastern Pacific (170°E - 90°W) for January 1986-July 1988. The thick contours represent total **ISHC**. They start from 10 W m^{-2} and increase by an interval of 10 W m^{-2} . The thin contours represent total SST. They start at 24°C and increase by an interval of 2°C . The areas where total SSTs are warmer than 28°C are shaded dark gray. (b) As in (a) but the thin contours and shadings are for total surface wind divergence. The thin dashed contours indicate convergence and the thin solid contours indicate divergence. Thin contours start from $\pm 1 \times 10^{-6} \text{ s}^{-1}$ and increase or decrease by an interval of $2 \times 10^{-6} \text{ s}^{-1}$. The areas in which convergence is stronger than $1 \times 10^{-6} \text{ s}^{-1}$ are shaded by dark gray. The areas in which divergence is stronger than $1 \times 10^{-6} \text{ s}^{-1}$ are shaded by light gray.

Figure 7: (a) Monthly mean vertical profiles of θ_e (dashed curve with diamonds) and θ_{es} (solid curve with dots) at Tarawa Island in the equatorial central Pacific for May 1988. The unit for the horizontal axis is K, and for the vertical axis is mb. (b) As in (a) but for May 1987.

Figure 8: As in Figure 7 but for Pago Pago Island in the southern, central Pacific.

Figure 9: As in Figure 4 but for ISLC for the eastern Pacific and Atlantic oceans. The critical correlation coefficients at a 95% confidence level are ± 0.47 . The areas where correlations are significant are shaded. The equatorial, eastern Pacific (10°S - 10°N , 150°W - 80°W) is excluded

Figure 10: As in Figure 7 but for St. Helena Island in the south eastern Atlantic ocean.

Figure 11: (a) Map of linear regression coefficients between ISTO over the global tropical oceans and SSTN3 for July 1983-December 1990. The dashed contours represent positive regression coefficients and the solid contours represent negative regression coefficients. Contours start from $\pm 1 \text{ W m}^{-2}$ with intervals of 2 W m^{-2} . The areas with positive regression coefficients are shaded dark gray, and those with negative are shaded light gray. (b) As in (a) but for ISHC and SSTN3. Contours start from 2 W m^{-2} , with intervals of 4 W m^{-2} . (c) As in (a) but for ISLC and SSTN3 for the eastern Pacific and Atlantic oceans.

Figure 12: (a) Coherence between low frequency variations (7.5-45 months) of Q_s (-ISTO) and dT_s/dt over global tropical oceans for July 1983-December 1990. Contours start from 0.4 and increase by an interval of 0.2. The areas between 0.4-0.6 are shaded by light grey and those above 0.6 are shaded by dark grey. (b) As in (a) but for phase difference, The solid contours indicate Q_s leads dT_s/dt by 0° to 180° . The dashed contours indicate Q_s lags dT_s/dt by -180° to -45° . The contour interval is 45° . The areas with phase difference ranging from 0° to 90° are shaded.

Table I: The number of EOF modes and percentage of the total variance retained in the reconstruction.

Variable	#of modes	variance
ISTO	23	53%
ISHC	7	32%
ISMC	12	43%
ISLC	16	63%
FDC	16	47%
SST	23	84%
dT_s/dt	8	39%

a) total ISHC/ISTO, Annual Climatology, 1/86-12/90

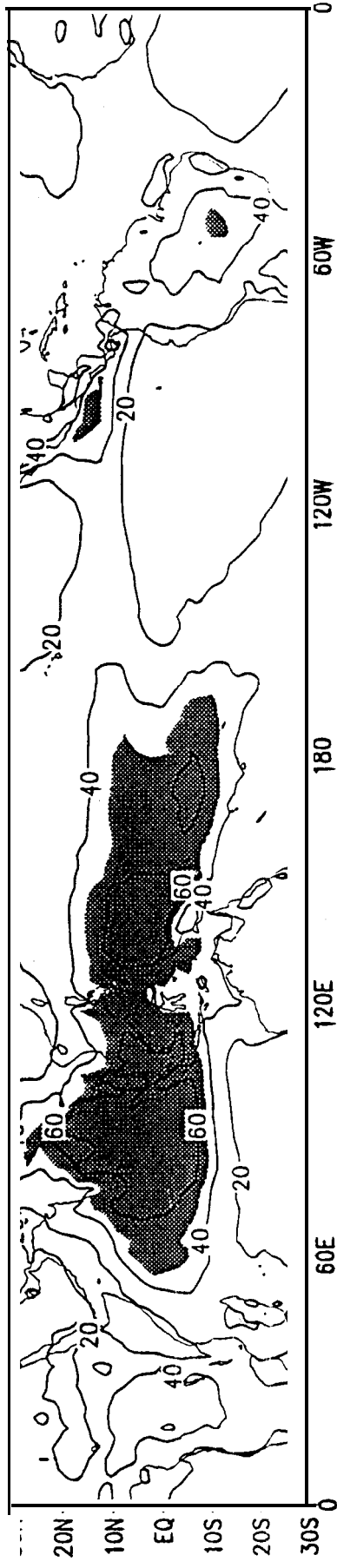


Fig.1

b) total ISMC/ISTO, Annual Climatology, 1/86-12/90

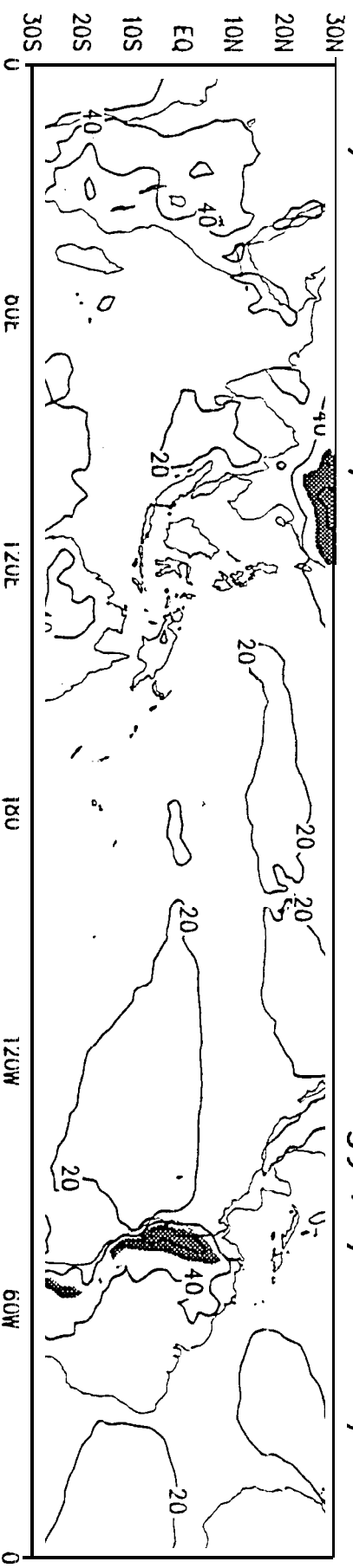


Fig. 2

c) total IS-C/ISTO, Annual Climatology 1/86-12/90

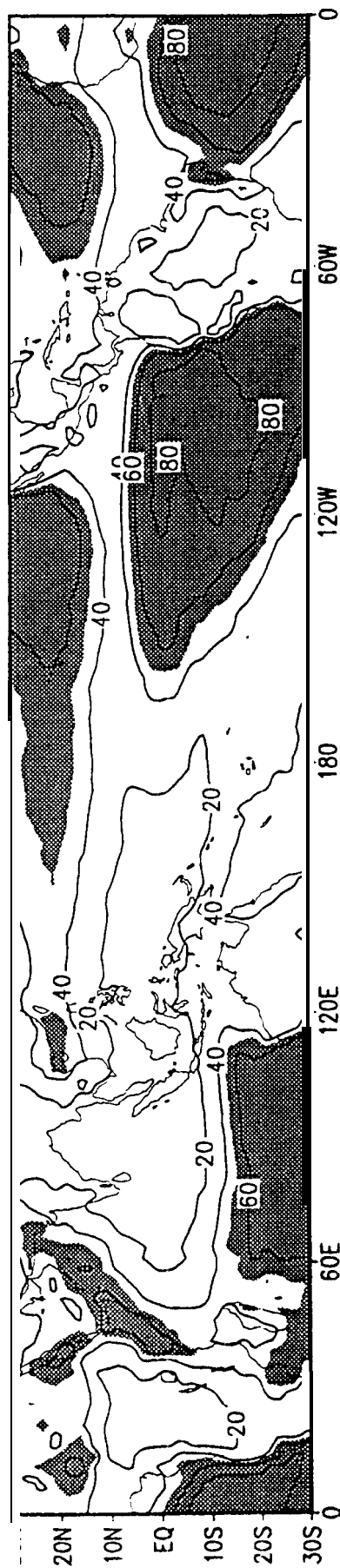


Fig.1

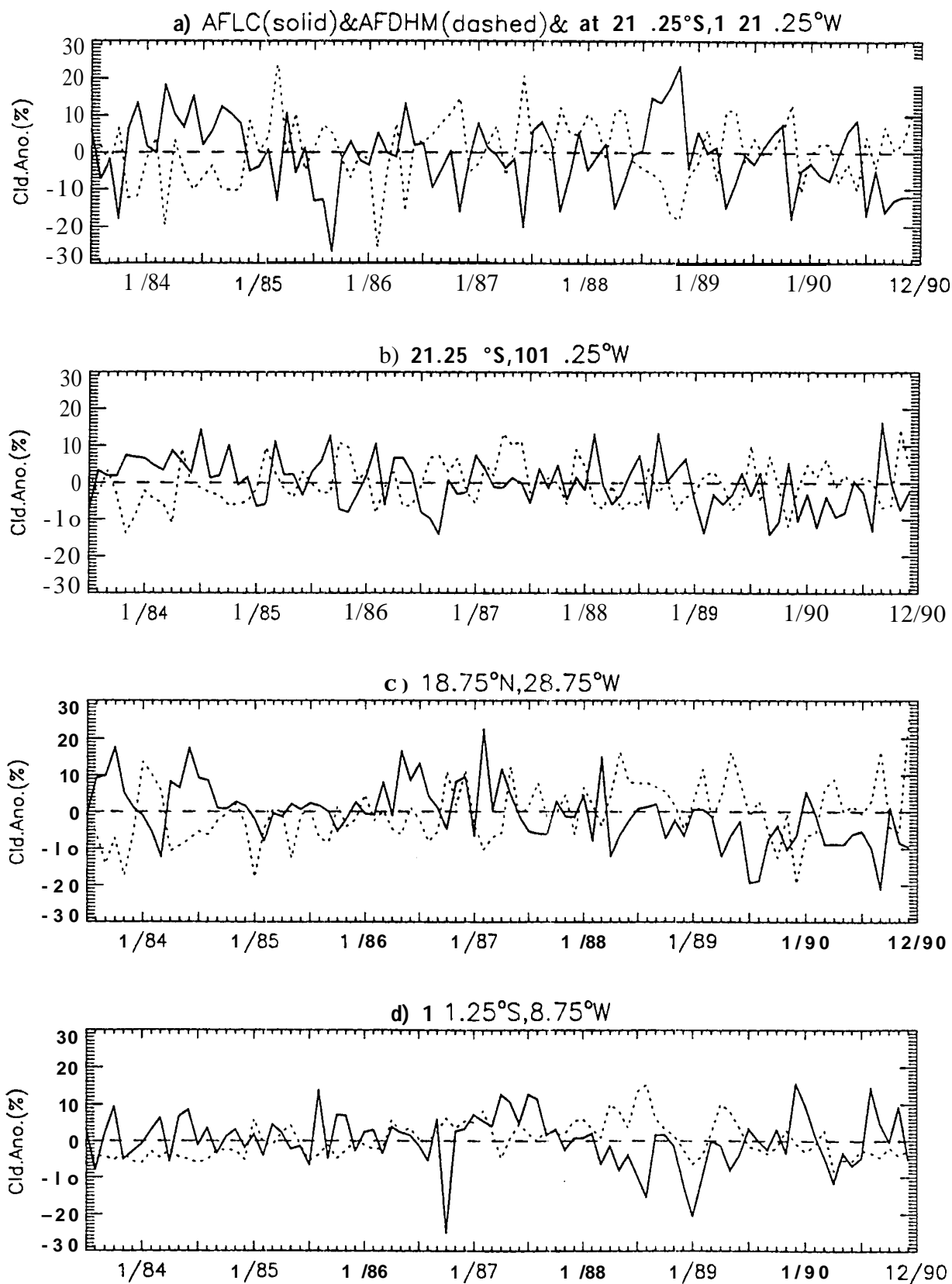


Fig.2

a) ISHC vs. IST0, $r_c=0.28, 7/83-12/90$

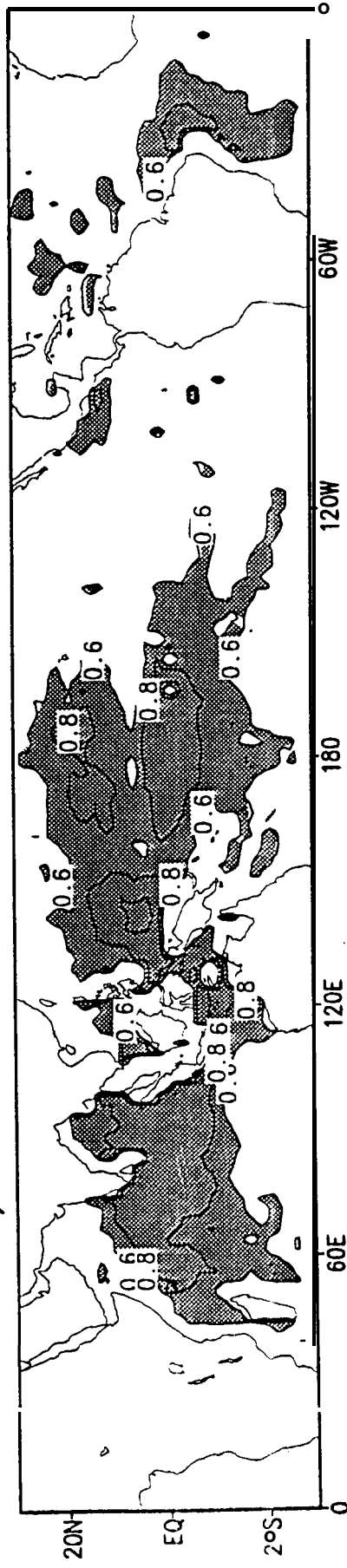


Fig 3

b) SMC vs. ISTO, $rc^{\circ} = 28, 7/83-12/90$

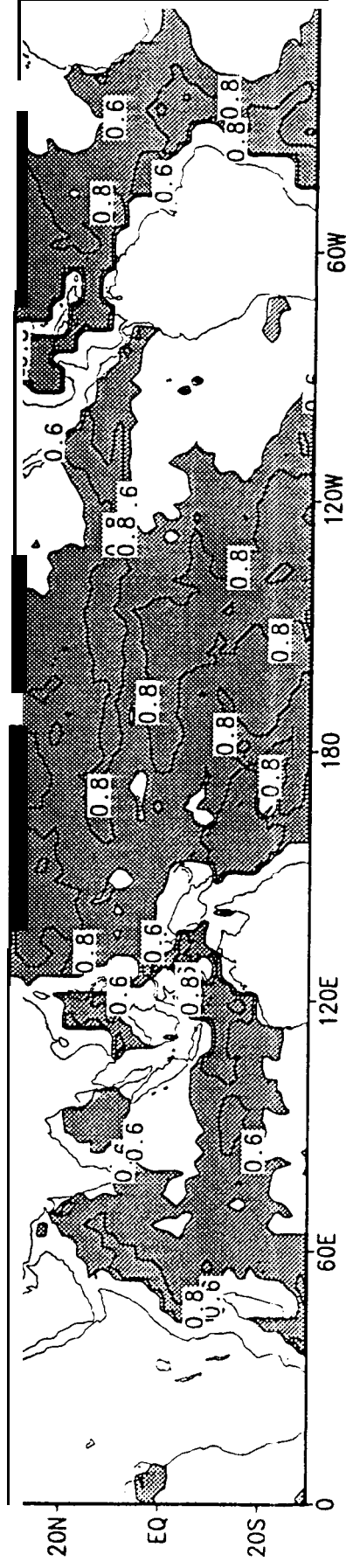


Fig. 3

c) IS-C vs. IST0, $r_c=0.28$, 7/83-12/90

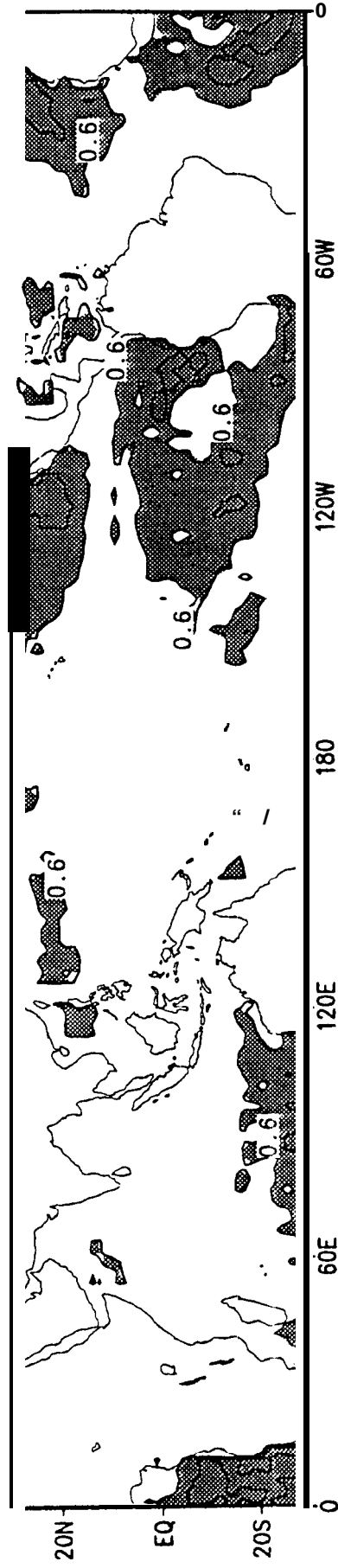
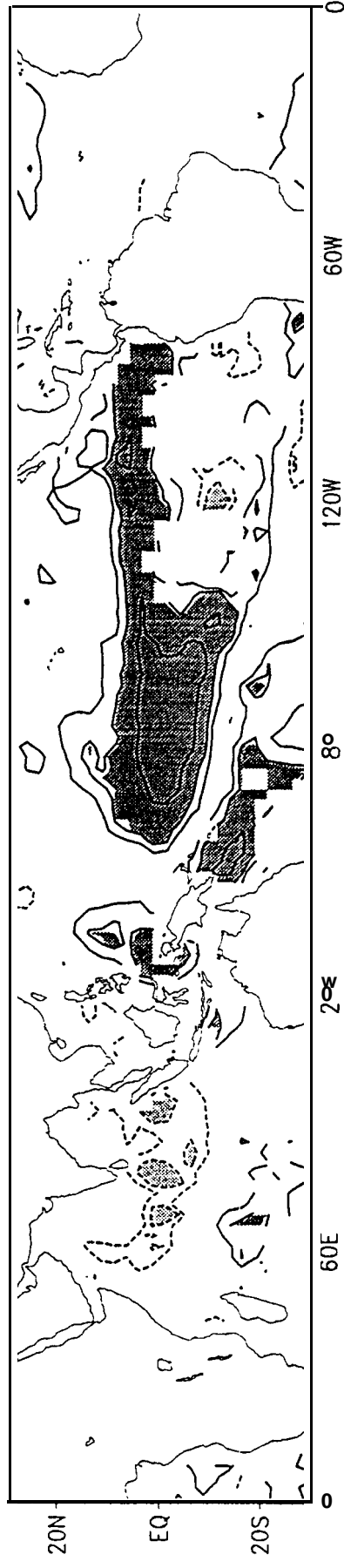


Fig. 3

c) SHC v.s. SST $rc=62$, 7/83-12/90



b) SHC v.s. SSTn3 $rc=62$, 7/83-2/90

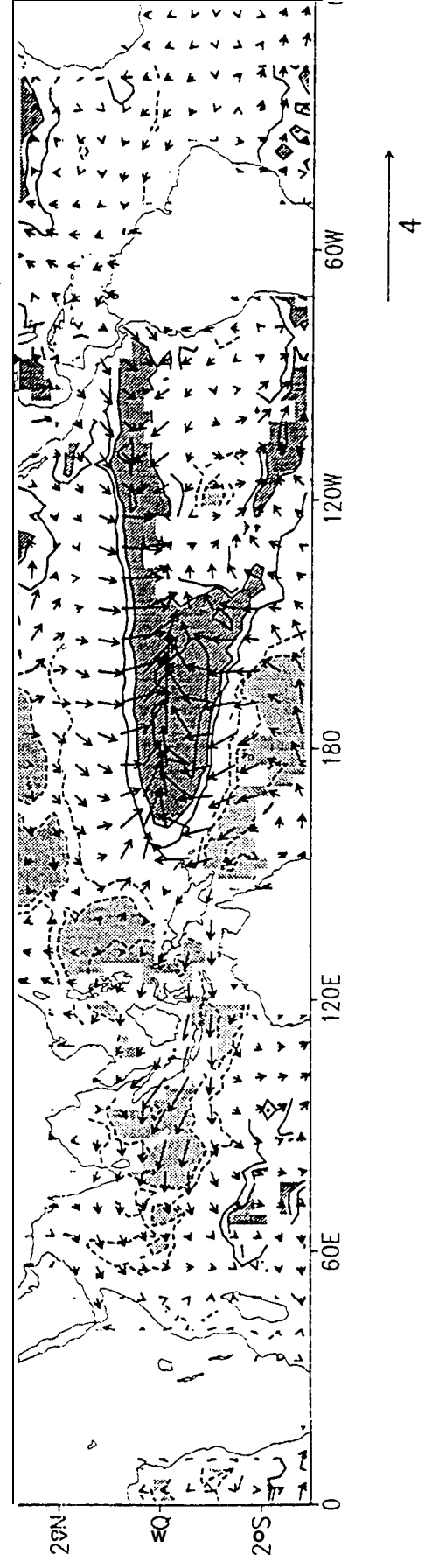
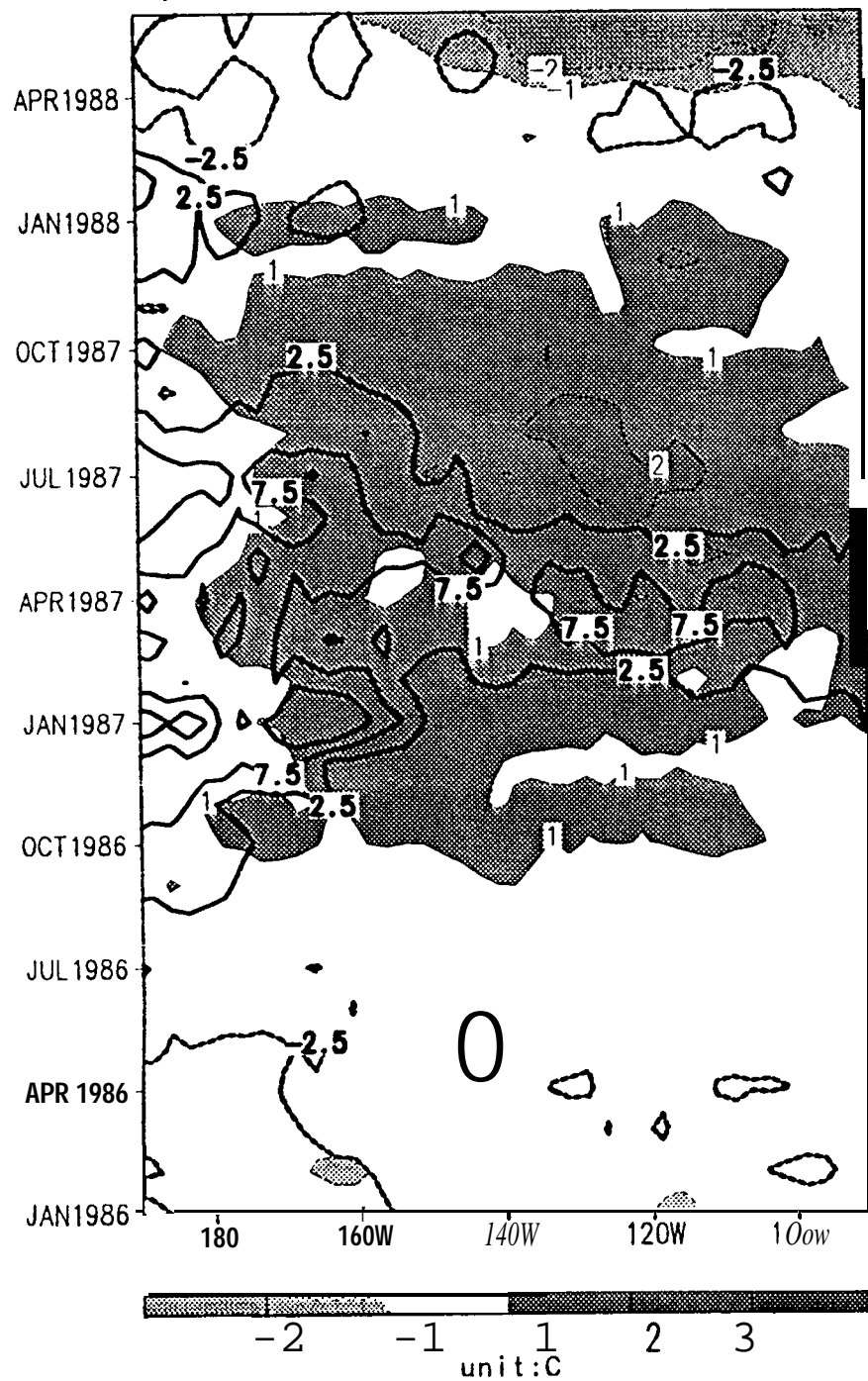


Fig.4

a) FDC and SST at 1.25N



b) ISHC and SST at 1.25N "

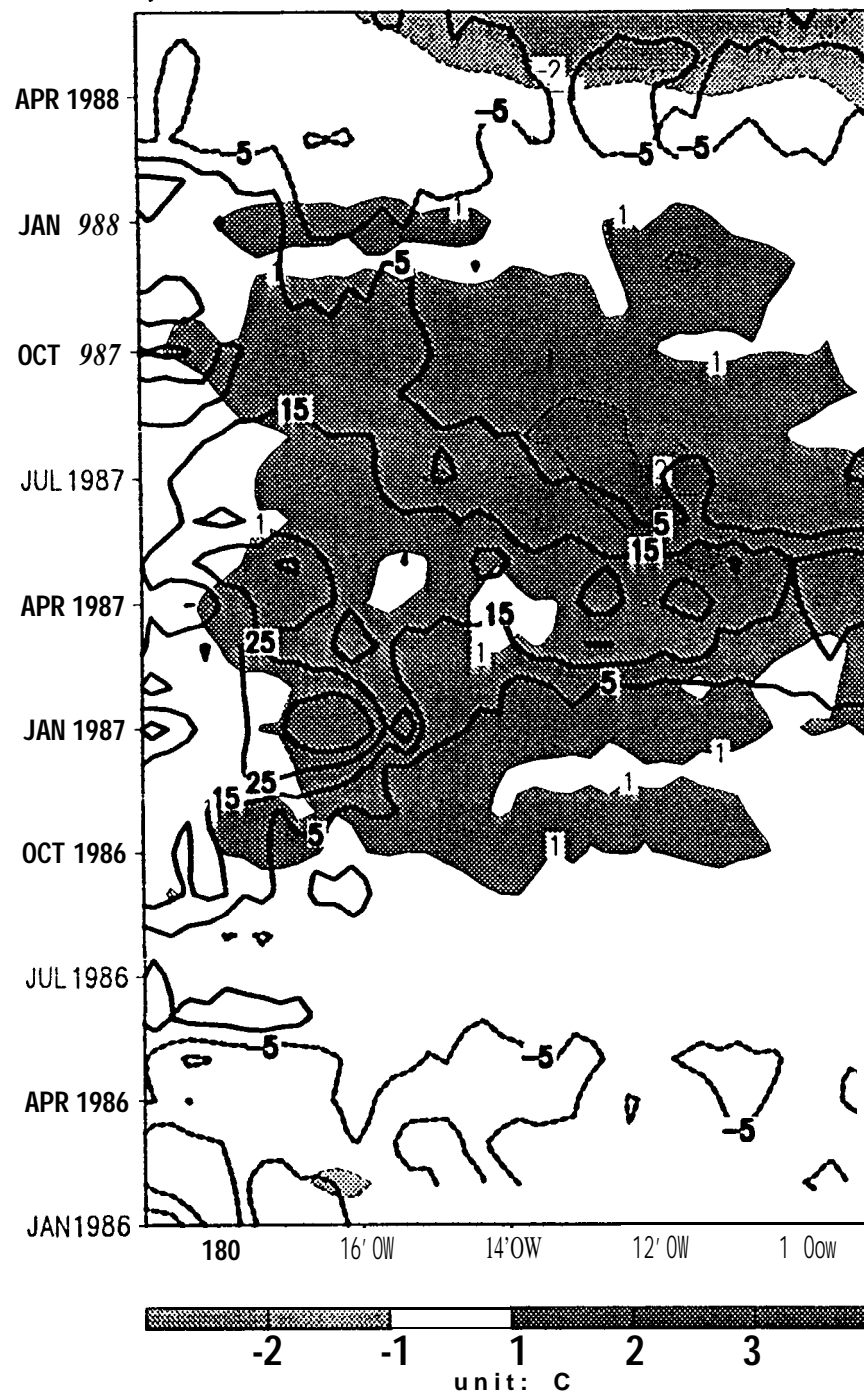
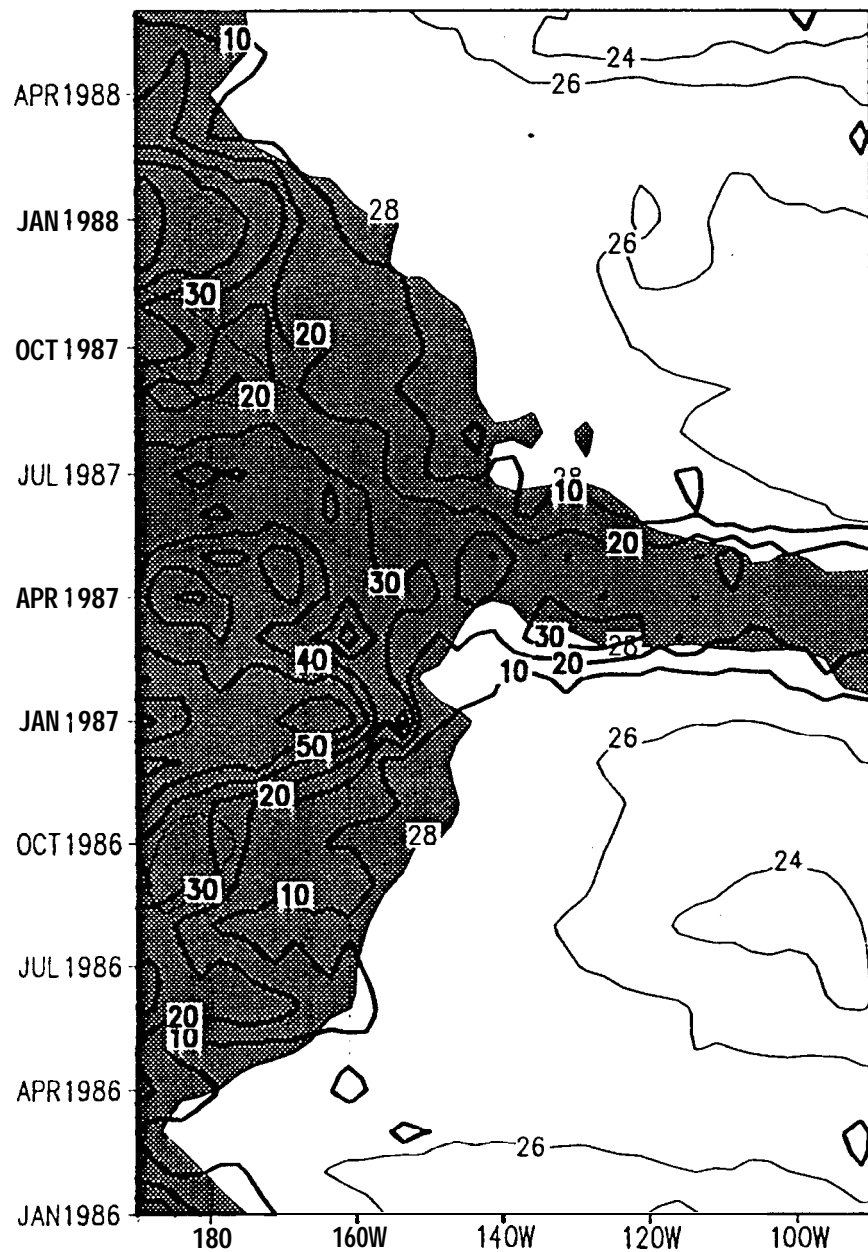


Fig. 5

a) ISHC and SST at 1.25N



b) ISHC and Div at 1.25N

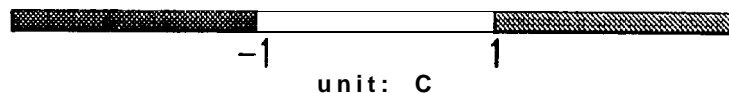
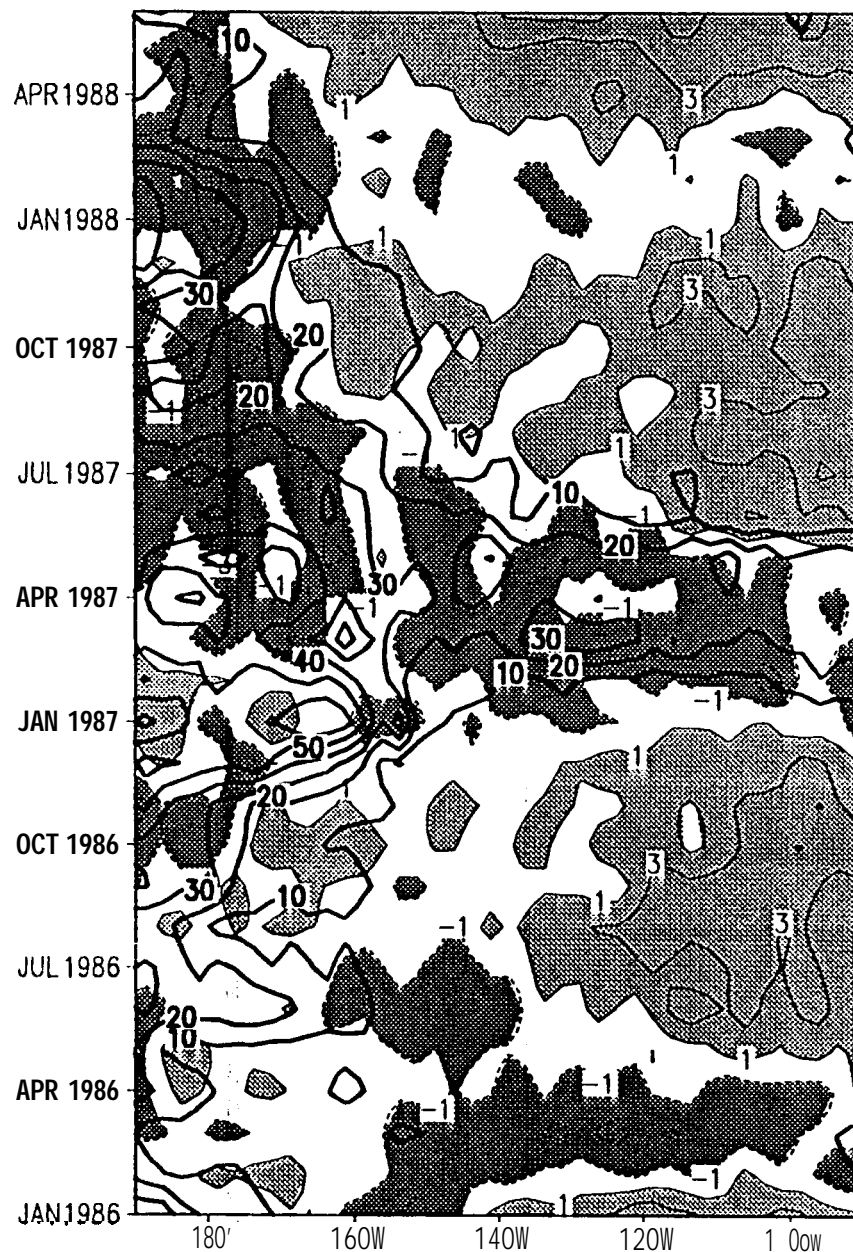


Fig. 6

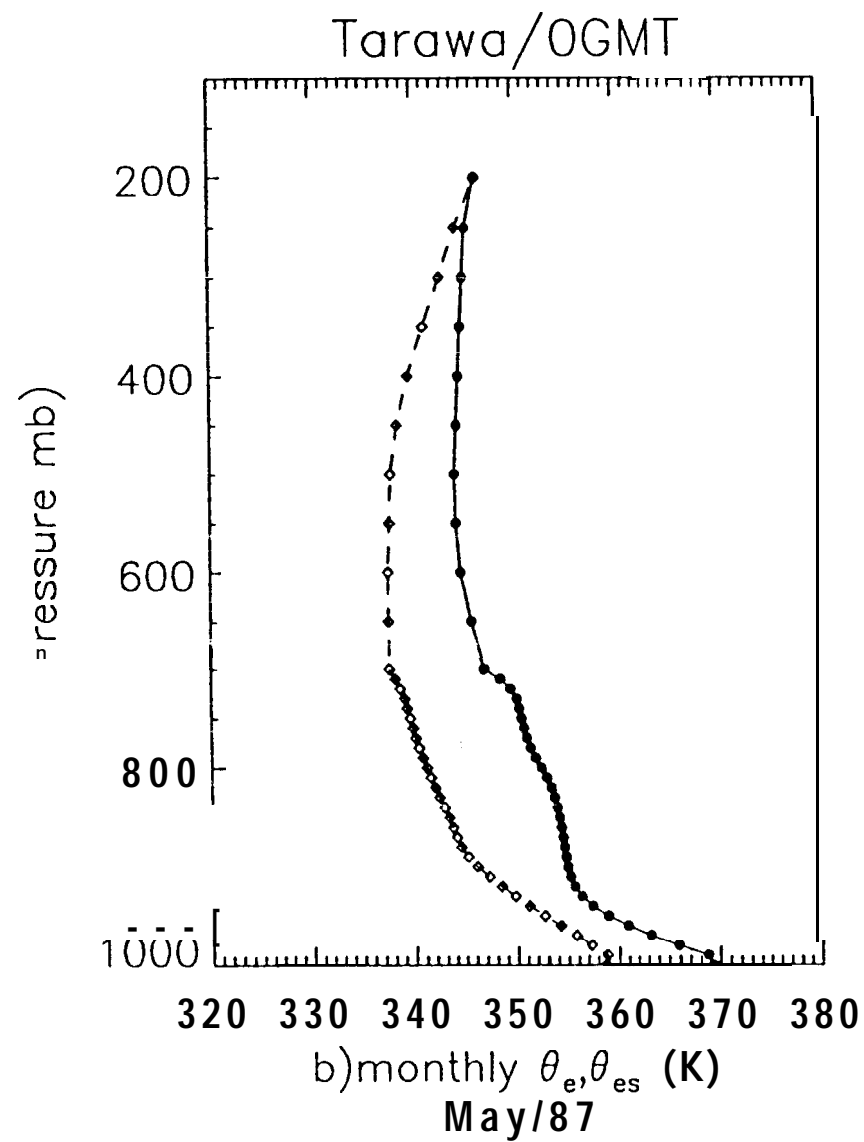
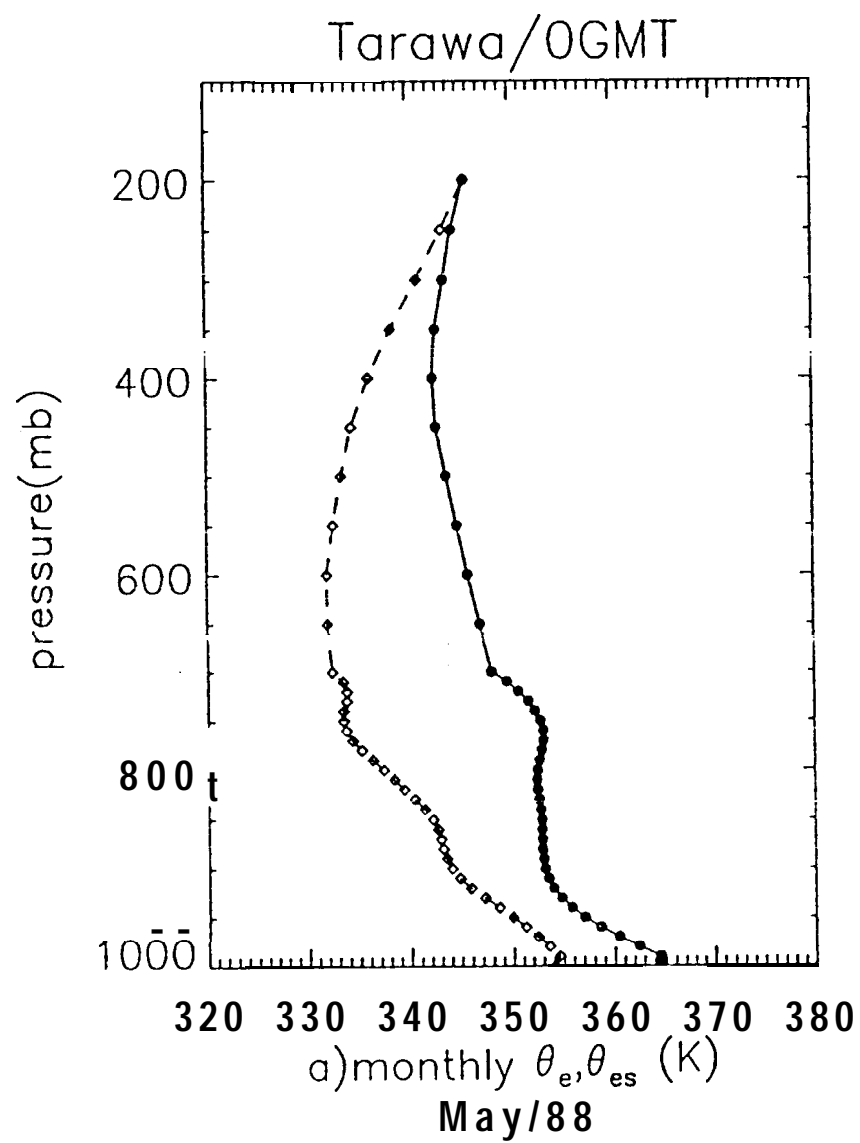


Fig.7

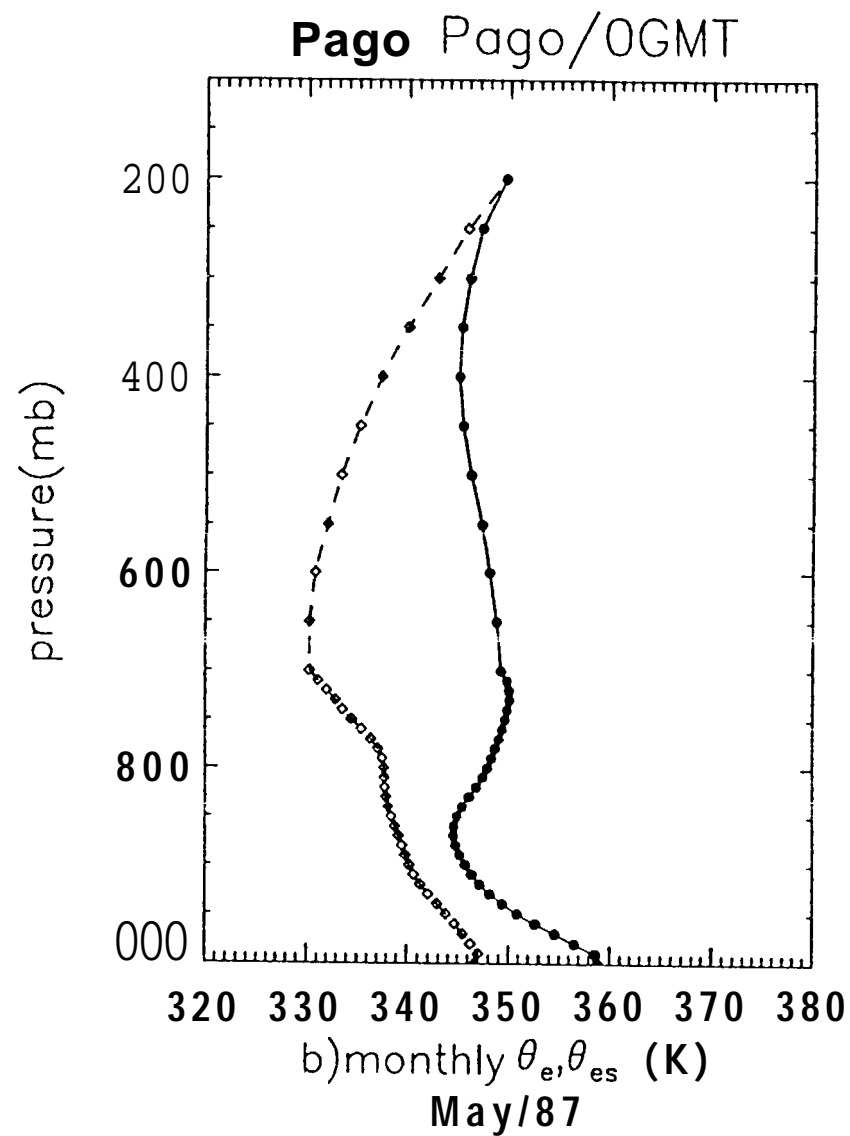
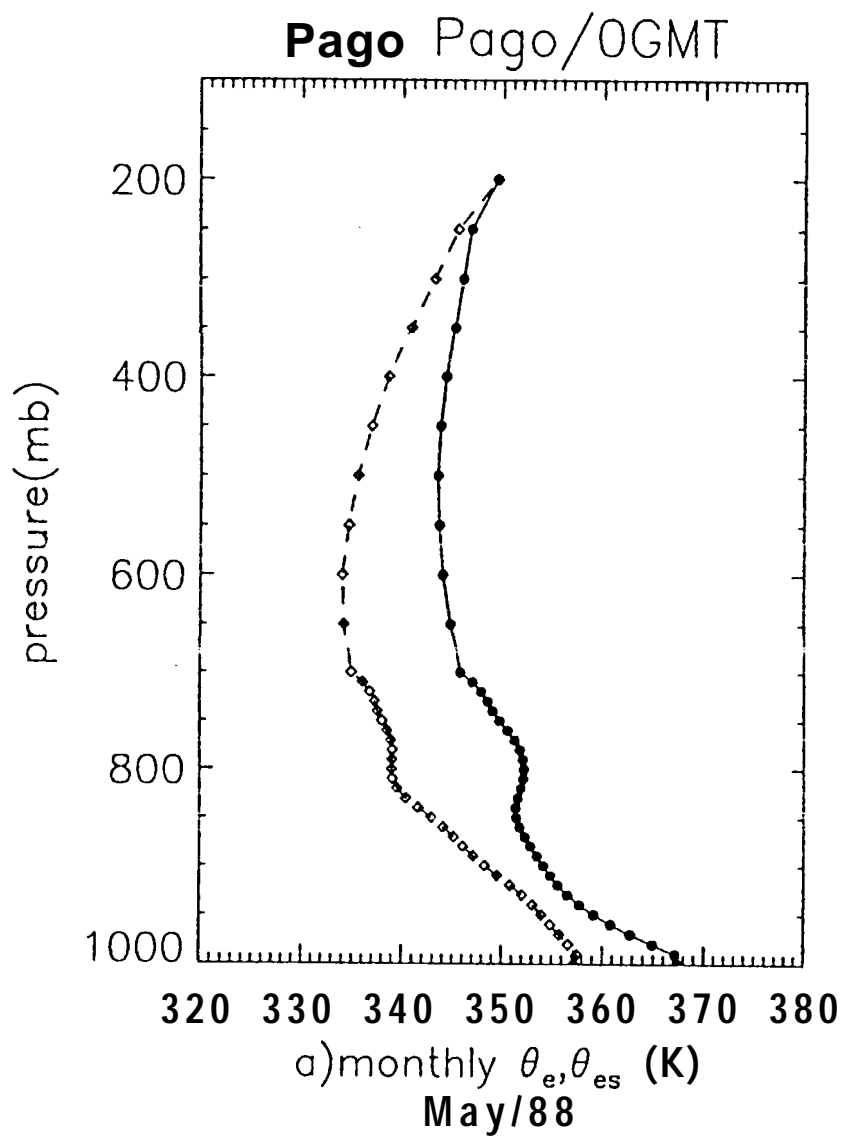
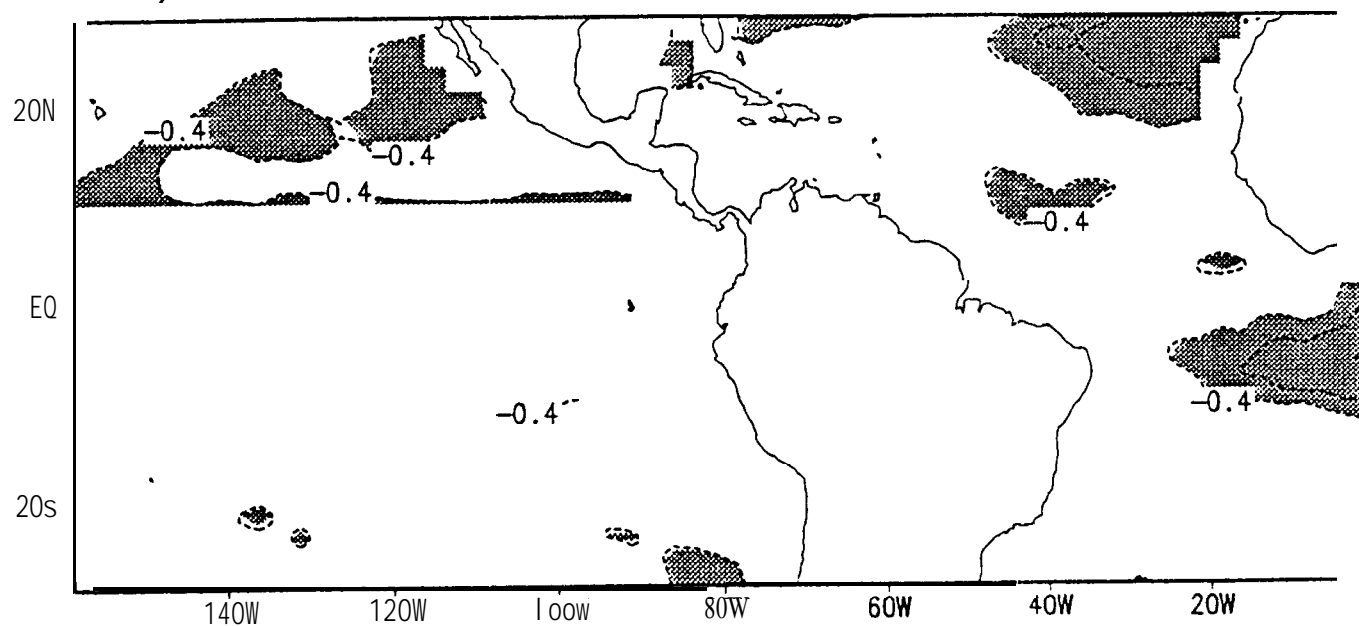


Fig.8

a) ISLC vs. SST, $rc=0.47$, 7/83-12/90



b) ISLC vs. SSTn3, $rc=0.47$, 7/83-12/90

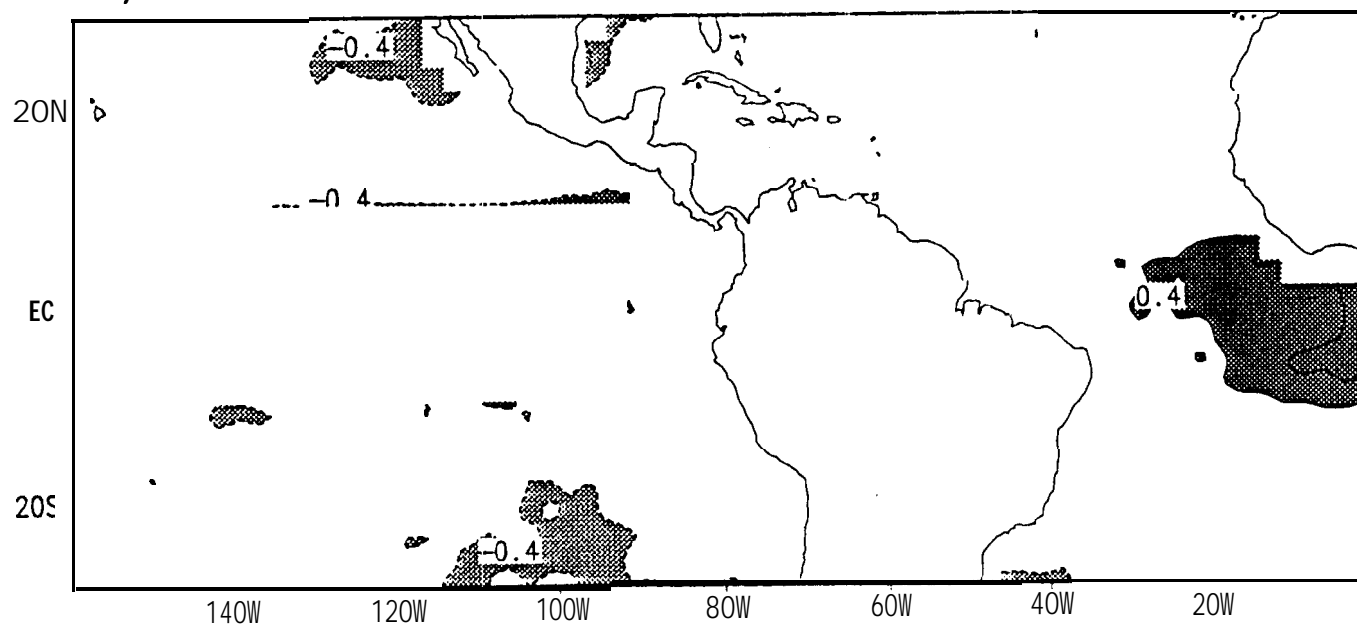


Fig. 9

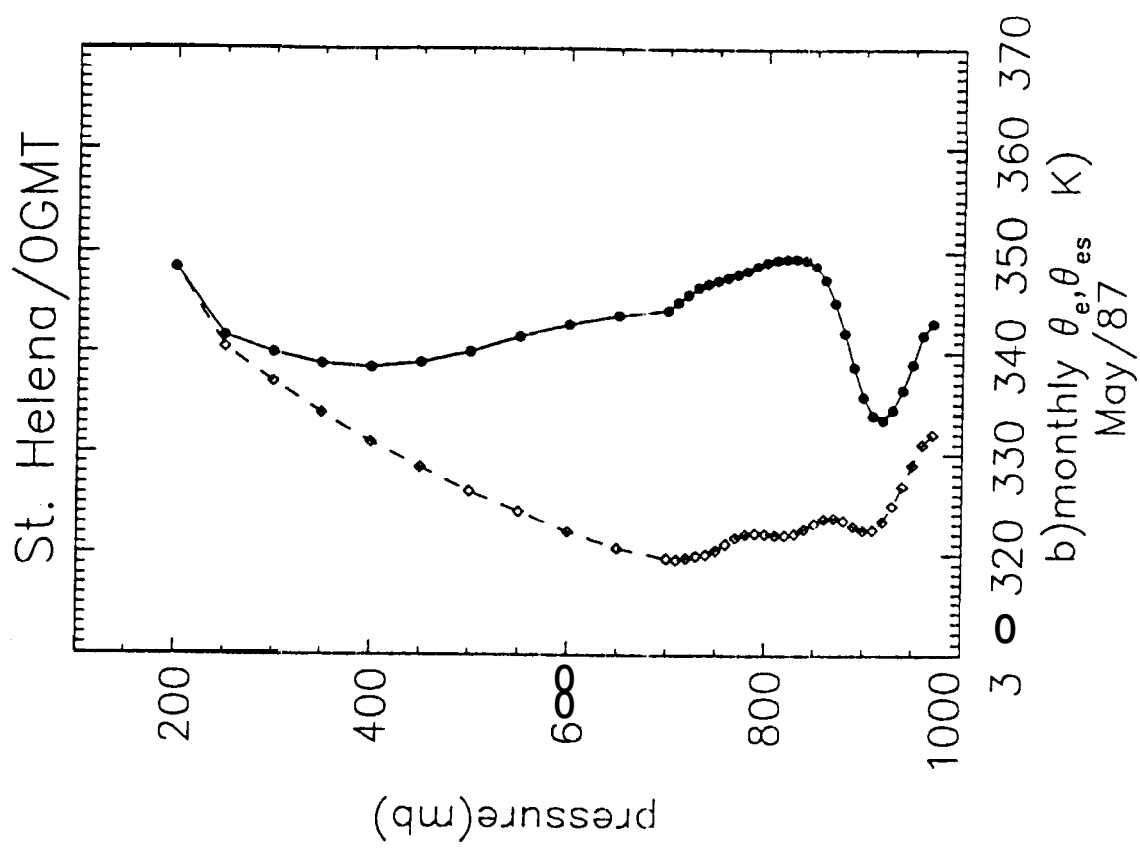
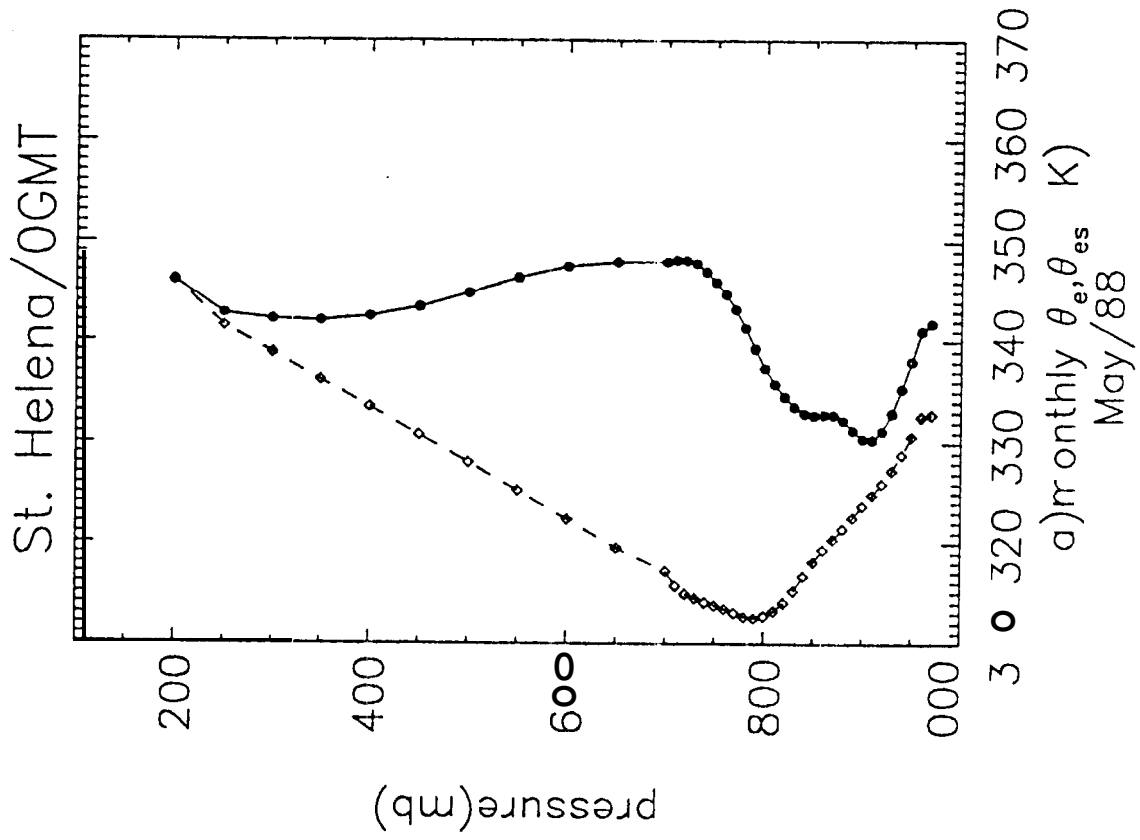
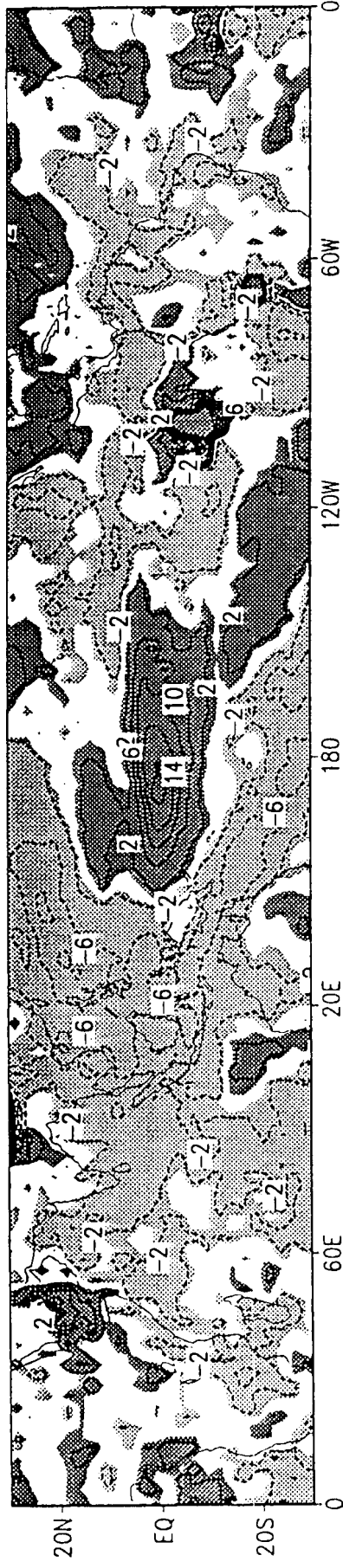


Fig.1°

a) ST0/SSTn3 4Wm**2/C, 7/83-12/90



b) SHC/SSTn3 4Wm * 2/C 7/83-12/90

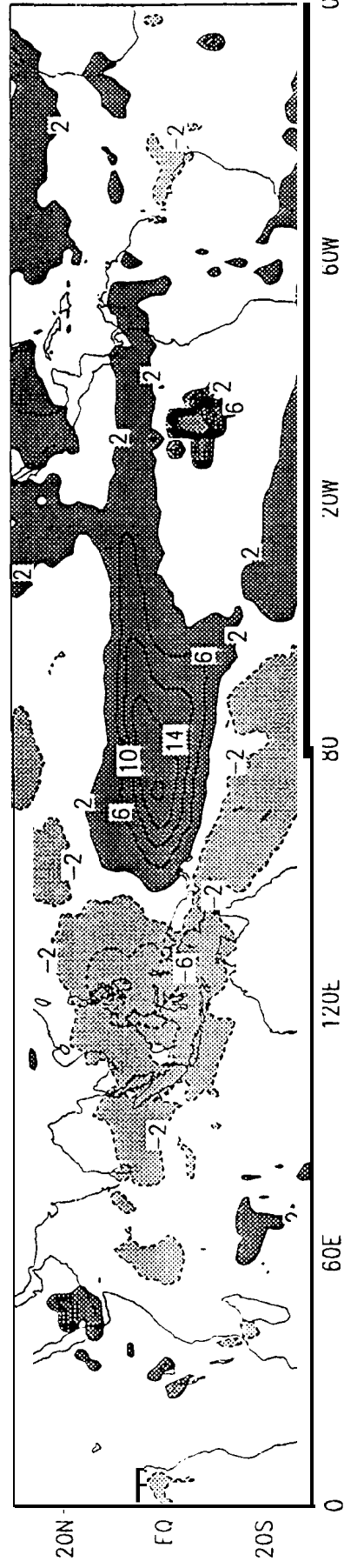


Fig. 11

c) SLC/SSTn3 2Wm**2/C 7/83-12/9^{eq}

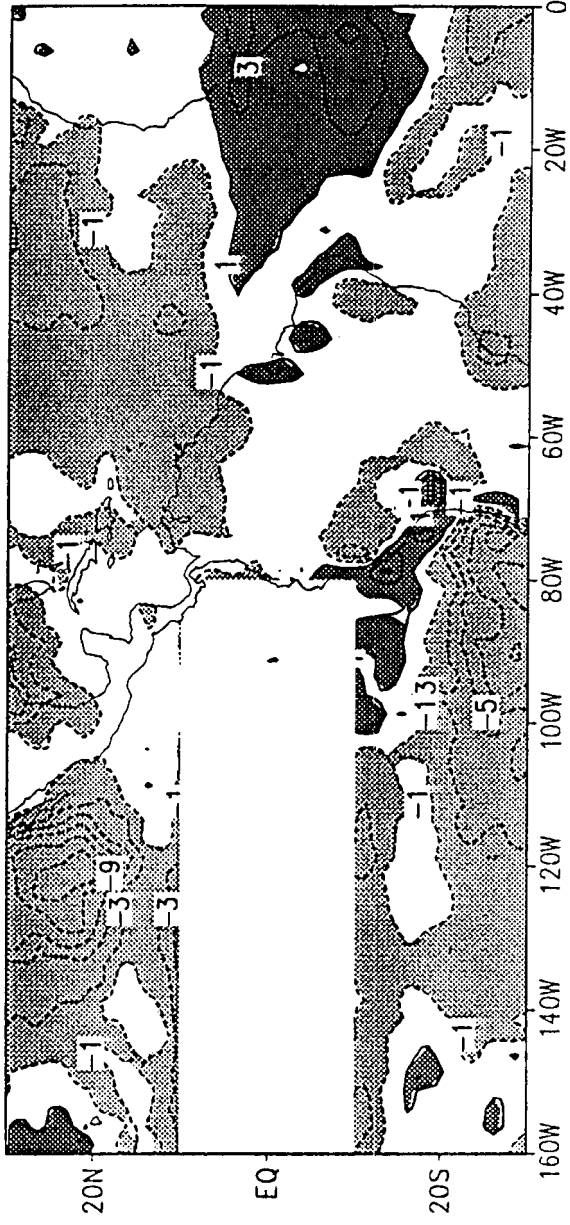
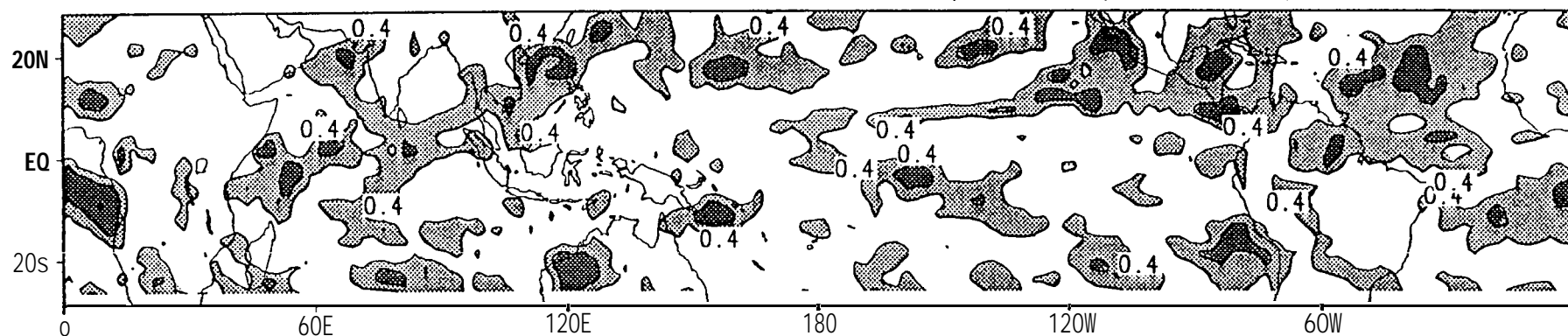


Fig.11

a) Coherence, Q_s vs. dT_s/dt , 7/83–12/90



b) Phase, Q_s vs. dT_s/dt , 7/83–12/90

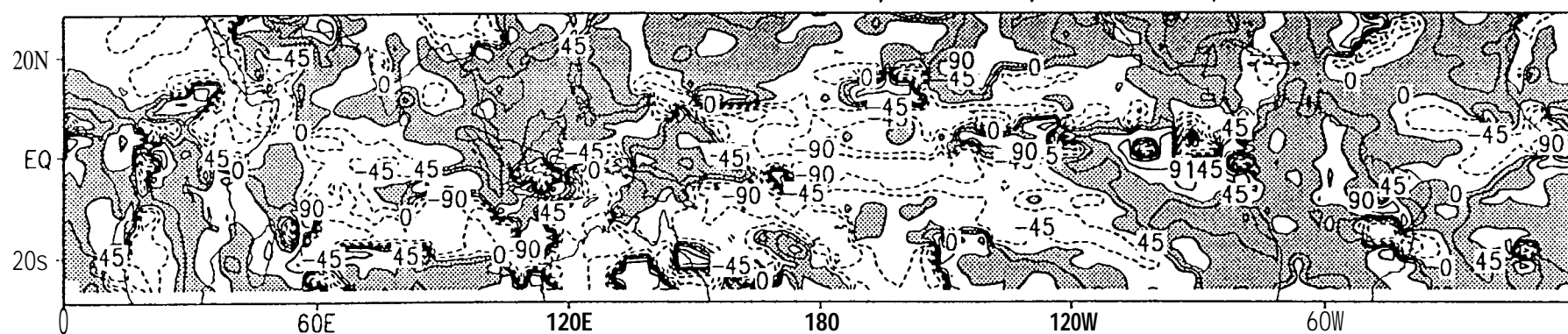


Fig. 12

